Constraints on the origin and evolution of Iani Chaos, Mars

Constraints on the origin and evolution of Iani Chaos, Mars

Nicholas H. Warner,[1] Sanjeev Gupta,[1] Jung-Rack Kim,[2,3] Jan-Peter Muller,[4] Lucille Le Corre,[4] Jeremy Morley,[5] Shih-Yuan Lin,[6] and Chris McGonigle[1]

Received 7 December 2010; revised 4 March 2011; accepted 18 March 2011; published 15 June 2011.

[1] The origin mechanisms and geologic evolution of chaotic terrain on Mars are poorly constrained. Iani Chaos, located at the head Ares Vallis, is among the most geomorphologically complex of the chaotic terrains. Its morphology is defined by (1) multiple, 1 to 2 km deep basins, (2) flat-topped, fractured plateaus that are remnants of highland terrain, (3) knobby, fractured remnants of highland terrain, (4) plateaus with a knobby surface morphology, (5) interchaos grooved terrain, (6) interior layered deposits (ILDs), and (7) mantling material. Topography, the observed geomorphology, and measured fracture patterns suggest that the interchaos basins formed as a result of subsurface volume loss and collapse of the crust, likely owing to effusion of groundwater to the surface. Regional patterns in fracture orientation indicate that the basins developed along linear zones of preexisting weakness in the highland crust. Multiple overlapping basins and fracture systems point to multiple stages of collapse at Iani Chaos. Furthermore, the total estimated volume loss from the basins (10^4 km^3) is insufficient to explain erosion of 10^4–10^5 km^3 of material from Ares Vallis by a single flood. Comparisons with the chronology of Ares Vallis indicate multiple water effusion events from Iani Chaos that span the Hesperian, with termination of activity in the early Amazonian. Recharge of groundwater through preexisting fracture systems may explain this long-lived, but likely episodic, fluvial activity. Late-stage, early to middle Amazonian aqueous processes may have deposited the ILDs. However, the topography data indicate that the ILDs did not form within lacustrine environments.

Citation: Warner, N. H., S. Gupta, J.-R. Kim, J.-P. Muller, L. Le Corre, J. Morley, S.-Y. Lin, and C. McGonigle (2011), Constraints on the origin and evolution of Iani Chaos, Mars, *J. Geophys. Res.*, *116*, E06003, doi:10.1029/2010JE003787.

1. Introduction

1.1. Origin of Chaotic Terrains

[2] The chaotic terrains on Mars consist of enclosed and semienclosed basins that are composed of, and are surrounded by, extensionally fractured cratered highland terrain [*Carr*, 1996, 1979; *Rodriguez et al.*, 2005a; *Scott and Tanaka*, 1986; *Tanaka et al.*, 2005]. For any given chaos region, the fractured highlands exhibit some morphologic variation between (1) densely fractured knobby terrain/conical mounds and (2) fracture bounded plateaus and mesas. The association of several chaotic terrains with outflow channels implies that these systems are closely related to a complex set of processes that caused massive evacuations of groundwater onto the surface and collapse of the crust [*Baker and Milton*, 1974; *Baker*, 1982; *Baker et al.*, 1991; *Carr*, 1979; *Masursky et al.*, 1977; *Rodriguez et al.*, 2005a; *Sharp*, 1973].

[3] Despite the relative certainty that groundwater played a major role in the geologic history of many chaotic terrains on Mars, the precise mechanism of groundwater release onto the surface and the long-term geologic evolution of individual chaos regions remain highly uncertain. Several plausible hypotheses for the cause of collapse at each chaos region have been suggested for both the chaotic regions that are associated with floods and those that are not. From image-based observations, hydrologic modeling, and observed mineralogical relationships (e.g., presence of sulfates) these hypotheses are as follows: (1) catastrophic release of water from deep (~1 to ~2 km) pressurized subsurface aquifers that were previously confined beneath a globally extensive, thick cryosphere [*Carr*, 1979; *Leask et al.*, 2006; *Lucchitta et al.*, 1994], (2) release of groundwater from confined subsurface caverns [*Rodriguez et al.*, 2003], (3) melting of subsurface or near-surface ice by an igneous intrusion or subaerial/subglacial volcanism [*Chapman and Tanaka*, 2002; *Chapman et al.*, 2003; *Leask et al.*, 2006; *Masursky et al.*, 1977; *Maxwell and Picard*, 1974; *Meresse et al.*, 2008], (4) release of

[1]Department of Earth Science and Engineering, Imperial College London, London, UK.
[2]Ziin Consulting, Seoul, South Korea.
[3]Now at Department of Geoinformatics, University of Seoul, Seoul, Korea.
[4]Mullard Space Science Laboratory, Department of Space and Climate Physics, University College London, Holmbury St. Mary, UK.
[5]Centre for Geospatial Science, University of Nottingham, Nottingham, UK.
[6]Department of Land Economics, National Chengchi University, Taipei, Taiwan.

0148-0227/11/2010JE003787

groundwater during major impact events [*Wang et al.*, 2005], (5) dewatering of hydrous minerals by subsurface heat (e.g., igneous intrusions) [*Kargel et al.*, 2007; *Montgomery and Gillespie*, 2005], (6) dissolution of subsurface hydrous clathrates [*Hoffman*, 2000; *Komatsu et al.*, 2000; *Max and Clifford*, 2001], (7) melting and collapse of buried water ice in a confined basin [*Zegers et al.*, 2010], and (8) sublimation of an ice-rich substrate [*Pedersen and Head*, 2010].

[4] It is unclear whether a single overarching mechanism can explain the formation of all chaotic terrains. Variation in the geomorphology of different chaos regions implies that different formation mechanisms may have operated. As an example, putative volcanic landforms that may suggest cryospheric melting and collapse are associated with some chaotic terrains, such as Hydraotes Chaos [*Meresse et al.*, 2008], but are lacking in other regions, like Aram Chaos [*Glotch and Christensen*, 2005]. In addition, chaotic terrains like Aromatum Chaos show evidence for only a single collapse event [*Leask et al.*, 2006], while others, including Aureum Chaos [*Rodriguez et al.*, 2005a], contain multiple overlapping basins that may require multiple collapse episodes.

1.2. Chronology of Chaotic Terrains

[5] A relative chronology for chaotic terrains on Mars has been established from comparisons with bulk crater model ages for the surrounding regions and associated outflow channels [*Rotto and Tanaka*, 1995; *Scott and Tanaka*, 1986; *Tanaka et al.*, 2005]. From these studies, there are generalized constraints on the timing of chaos formation on Mars. For the dense cluster of chaotic terrains in the circum-Chryse and Valles Marineris regions, the crater statistics indicate that they formed after the late Noachian to early Hesperian cratered highland terrain that they are contained within and that they are temporally related to early Hesperian to early Amazonian outflow activity. However, the complex relationships that likely exist between multiple flood events [*Andrews-Hanna and Phillips*, 2007; *Harrison and Grimm*, 2008; *Nelson and Greeley*, 1999; *Ori and Mosangini*, 1998; *Warner et al.*, 2009, 2010; *Williams et al.*, 2000] and chaos evolution have not been described through morphology and chronology. For example, while a chaos region that exhibits a single collapsed basin may be explained by a temporally punctuated and geologically unique event, such as melting of the cryosphere by a volcanic intrusion, chaotic terrains that show multiple collapse zones with multiple issuing flood channels may require a multiphase or longer-term collapse-inducing process.

1.3. Iani Chaos

[6] As a prime example of a morphologically complex chaotic terrain, Iani Chaos (Figure 1) is located east of Valles Marineris, at the northern margin of Margaritifer Terra and at the head of Ares Vallis, centered at 2.0°N, 342.2°E. The entire chaos region is ~400 km wide and contains a series of semienclosed basins that are composed of, and are surrounded by, fractured plateaus and knobby terrain. The morphology of the region and location at the head of Ares Vallis has been used to suggest that Iani Chaos formed by collapse following the catastrophic release of groundwater [*Andrews-Hanna and Phillips*, 2007; *Grant and Parker*, 2002; *Komatsu and Baker*, 1997; *Nelson and Greeley*, 1999; *Rodriguez et al.*, 2005a; *Tanaka et al.*, 2005].

[7] The morphologic complexity of the Iani Chaos system and previous lack of regional high-resolution data has meant that our understanding of its origin and geologic evolution is poorly constrained. Detailed topographic and morphologic characterization is now possible given the suite of regionally extensive high-resolution imagery and topography data made available by NASA's Mars Reconnaissance Orbiter (MRO) and ESA's Mars Express (MEX). In this analysis we present a topographic, geomorphologic, and chronologic study of the Iani Chaos system using new imagery and topography data sets to constrain its origin and geologic evolution as they relate to catastrophic flood events in Ares Vallis.

[8] Importantly, new data have revealed the likelihood that multiple smaller magnitude flood events carved the Ares Vallis flood system [*Andrews-Hanna and Phillips*, 2007; *Warner et al.*, 2009, 2010]. Using high-resolution crater statistics coupled with high-resolution topography, *Warner et al.* [2009] concluded that proximal Ares Vallis was the site of at least two and possibly six unique flood events that emanated from Iani Chaos and occurred from the early Hesperian (3.6 Ga) [*Hartmann and Neukum*, 2001] into the early Amazonian (2.5 Ga). From numerical hydrologic modeling, *Andrews-Hanna and Phillips* [2007] suggested that dozens of floods, resulting from a repeated succession of freezing and pressurized release of a subsurface aquifer, emanated from Iani Chaos and carved Ares Vallis. In addition, this study hypothesized that late-stage ponding of water may have led to deposition of the light-toned, interior layered deposits (ILDs). These proposed lacustrine environments may have been present at the sites of specific collapse depressions within Iani Chaos. Recently, the primary interest in this region of Mars has been on the ILDs, largely owing to orbital detections of hydrated minerals (e.g., hematite, sulfates) and the implications they hold for the past presence of surface aqueous environments that are of astrobiological interest [*Dobrea et al.*, 2008; *Gendrin et al.*, 2005; *Glotch and Rogers*, 2007].

[9] In this study, we demonstrate that the morphology of Iani Chaos evolved through intermediate stages in response to multiple releases of groundwater during the Hesperian and early Amazonian. Furthermore, our results show that groundwater must have been recharged from distal sources, suggesting a regionally extensive, connected aquifer. We describe a pattern in the basin and fracture morphology that indicates localized, fracture-controlled subsidence of the crust. This pattern may have been controlled by a preexisting condition of regional extensional stress that allowed groundwater to be recharged into Iani Chaos and released from discrete locations. Finally, we constrain both the timing of chaos formation and ILD deposition relative to flooding in Ares Vallis and suggest that the ILDs could not have formed within lacustrine environments.

2. Methods

2.1. Data Description

[10] High-resolution imagery and topography data were used to quantify the morphologic characteristics of chaos-related fractures, chaos blocks, interchaos flood surfaces, and interchaos basins. For the topographic analysis we con-

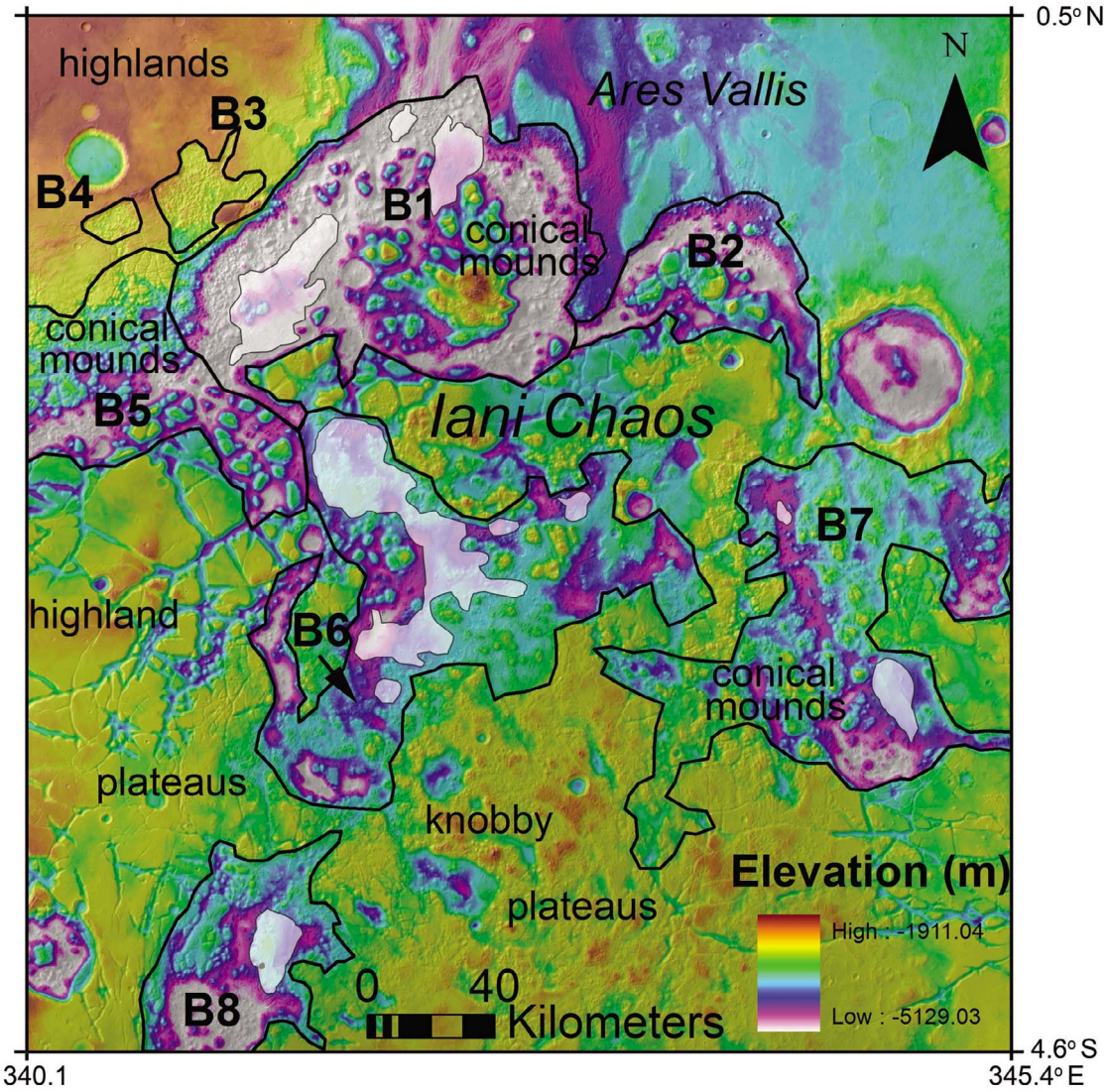

Figure 1. HRSC DTM (40 m) overlain by a 15 m HRSC orthoimage displaying the Iani Chaos region on Mars. The interchaos basins (B1–B8) and important morphologic features (e.g., highland plateaus, knobby plateaus, and conical mounds) are highlighted. Interior layered deposits (ILDs) are displayed in white.

structed a regional MEX High-Resolution Stereo Camera (HRSC) digital terrain model (DTM) with 40 m grid spacing by mosaicing six HRSC DTM orbital strips. The DTM construction methods developed at University College London have been previously described by *Kim and Muller* [2009] and *Warner et al.* [2009]. We also generated a near-complete georeferenced and map-projected MRO Context Camera (CTX) mosaic at 6 m pixel^{-1} of the chaos region to analyze the regional geomorphology. Specific geomorphic surfaces were mapped from the CTX mosaic (including the ILDs) to determine relative and absolute chronology by impact crater statistics. HRSC orthoimages (15 m pixel^{-1}) and the CTX mosaic were overlain on the digital terrain models to directly relate surface features to topography. Where available, MRO High-Resolution Imaging Science Experiment (HiRISE) images at 25 cm pixel^{-1} were obtained to highlight the stratigraphic characteristics of chaos blocks and the ILDs.

2.2. Impact Crater Chronology

[11] Previous crater counts from the highland terrains that surround Iani Chaos and Ares Vallis were acquired from Viking Orbiter and Mars Orbiter Camera (MOC) images using craters with diameters (D) > 2 km or D > 5 km [*Marchenko et al.*, 1998; *Nelson and Greeley*, 1999; *Rotto and Tanaka*, 1995; *Scott and Tanaka*, 1986; *Tanaka and Skinner*, 2004]. Crater model ages for the highlands suggest a late Noachian to early Hesperian (*Hartmann and Neukum* [2001] production function system, 4.0 Ga to 3.7 Ga) formation age. The timing of flood resurfacing in Ares Vallis has more recently been dated to the early Hesperian to early Amazonian periods (3.6 Ga to 2.5 Ga) [*Warner et al.*, 2009, 2010]. To improve upon these previous crater statistics studies we conducted high-resolution crater counting (D > 50 m for the ILDs, D > 100 m) and used absolute dating techniques established by *Hartmann and Neukum* [2001] to estimate the crater retention age of the prechaos highland

Table 1. Measured Volume and Depths for Individual Basins in Iani Chaos Measured From the 40 m HRSC DTM

Chaos Basin	Sum of Difference From TIN[a] (km)	Grid Area[b] (km^2)	Max Depth (km)	Mean Depth (km)	Volume (km^3)
B1	3804081	0.0016	1.9	0.7	6087
B2	686441	0.0016	1.3	0.4	1098
B3	92259	0.0016	0.6	0.2	148
B4	16384	0.0016	0.4	0.2	26
B5	931777	0.0016	1.5	0.4	1491
B6	1708856	0.0016	1.5	0.3	2734
B7	2064412	0.0016	1.1	0.3	3303
B8	605826	0.0016	1.5	0.3	969
Total					15856

[a]TIN, Triangulated Irregular Network.
[b]Single cell size equals 0.040 km.

terrain surrounding Iani Chaos, proposed sedimentary infill deposits (including the ILDs and mantling deposits), crater infill material, and interchaos flood surfaces.

[12] Counts were obtained from full-resolution CTX mosaics (6 m $pixel^{-1}$) using the Mars Editing and Assessment toolset [*Simpson et al.*, 2008]. This Visual Basic® application allows craters to be tagged and measured on an image backdrop, while saving relevant diameter and location data to an ESRI® shape file. The freeware program Craterstats was used to plot the crater statistics and to fit isochrons (with error) to estimate absolute ages [*Michael and Neukum*, 2008]. Crater statistics are presented here in table form as crater densities for N(0.05) (ILDs only), N(0.1), N(0.5), N(1), N(5) (where N represents the cumulative number of craters counted per 10^6 km^2) and on $\log_{10}$ cumulative frequency plots that utilize the production functions of *Ivanov* [2001] and chronology functions developed by *Hartmann and Neukum* [2001]. Wherever applicable, resurfacing corrections were made following *Michael and Neukum* [2010].

3. Observations and Results

3.1. Geomorphology of Iani Chaos

[13] Figure 1 displays the 15 m $pixel^{-1}$ HRSC image mosaic overlain on the 40 m HRSC DTM. Using these high-resolution regional data sets, we have classified Iani Chaos into general morphologic zones that we refer to throughout the analysis. These zones are delineated on the basis of characteristics of topography, relative chronology, fracture density, block morphology, and presence of geomorphic features that suggest water flow (e.g., flood grooves, channels, and streamlined remnants) and include (1) irregular, semicircular, or quasi-linear basins (B1–B8) (Figure 1), (2) fractured remnants of cratered highland terrain composed of horizontally layered bedrock, capped by a single, smooth resistant capping unit (highland plateaus), (3) fractured knobby terrain composed of isolated conical mounds that lack a resistant capping unit and contain subhorizontally layered bedrock, (4) fractured plateaus of cratered highland terrain composed of horizontally layered bedrock, exhibiting a knobby surface morphology (knobby plateaus), (5) grooved terrain that occurs between and issues from isolated topographic depressions, (6) ILDs that overlie fractures and chaos blocks and occur in isolated patches within or at the edge of the basins (Figure 1), and (7) mantling material that occurs throughout and beyond the spatial extent of Iani Chaos.

3.1.1. Interchaos Basins

[14] Figure 1 outlines the eight large (15 km to 120 km wide) basins (B1–B8) that form interconnected and isolated topographic lows throughout Iani Chaos. These basins were delineated on the basis of differences in total depth, planform morphology, orientation, and relative relationships to Ares Vallis flood terrain (where applicable). Table 1 highlights important morphometric and topographic characteristics of each basin. Below we provide a brief description of each basin.

[15] Basin 1 (B1) is the largest single basin within Iani Chaos. Located immediately south, and adjacent to the topographically lowest flood channel in Ares Vallis [*Warner et al.*, 2009], B1 can be best described as a semicircular ring basin, containing a densely fractured, central topographic rise that is composed of smooth, flat-topped blocks that are tens of kilometers wide and are on average 2 km high relative to the minimum elevation of the floor of the basin. The maximum elevation of the blocks that comprise the central high is −2230 m and is comparable to the elevation of the nonfractured highland terrain at the northwest margin of Iani Chaos (−2200 m) (Figure 2a). Interior layered materials (ILDs) are present in discrete patches in the north, east, and southwest portions of the basin (section 3.1.6) (Figure 1).

[16] Basin 2 (B2) is located east of B1 and heads the eastern branch of Ares Vallis [*Warner et al.*, 2009] (Figure 1). B2 is a semicircular ring basin that contains a fractured central high at ~1.7 km above the floor of the basin. The maximum elevation of the central high, at −2700 m, is comparable to cratered highland terrain located east of Iani Chaos (Figure 2b).

[17] Basins 3 and 4 (B3 and B4) are shallow depressions located along the northwest margin of Iani Chaos (Figure 1). Both depressions contain hundreds of 100 m scale conical mounds (Figure 2c). B3 is at its deepest ~600 m deep. To the south, B3 is crosscut by the topographically lower and younger interchaos basin, B5. B4 is separated from B3 by a 6 km wide block of nonfractured cratered highland terrain. B4 has a maximum depth of ~400 m. Located both adjacent to B3 and several kilometers west of B4, we have identified two unique grooved surfaces that are associated with shallow chaos depressions that are examples of interchaos flood terrain (see section 3.1.5) (Figure 3).

[18] Basin 5 (B5) is a quasi-linear topographic depression (east-northeast strike) located west of B1 (Figure 1). It has a maximum depth of ~1.5 km (Figure 2d). B5 is bounded to the north by shallow chaotic terrains associated with B3 and B4

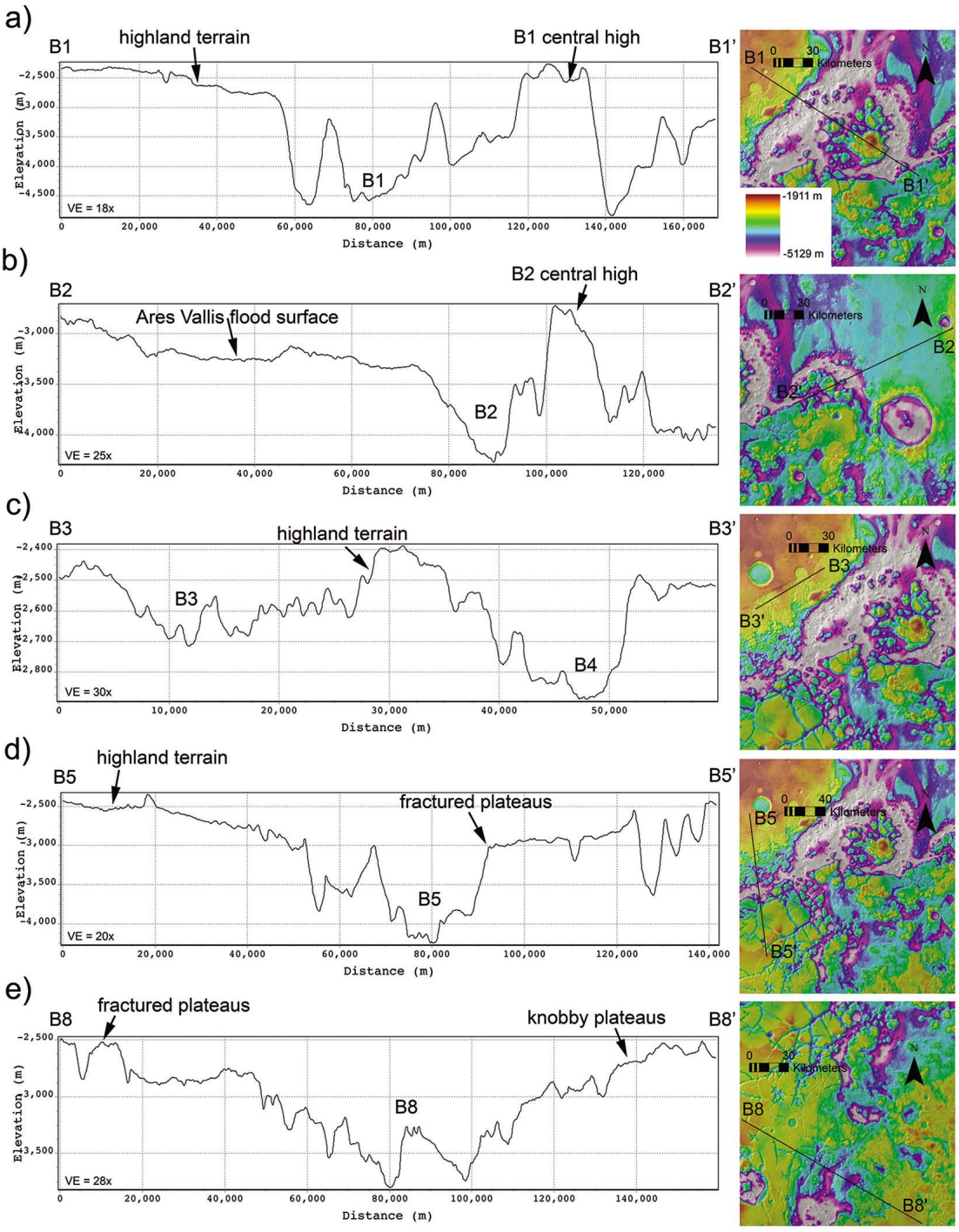

Figure 2. Topographic profiles derived from the 40 m HRSC DTM displaying the relative heights of the interchaos basins to the surrounding highland terrain. The basins are between 400 m and 2 km deep, relative to the highland terrain. The fractured plateaus that both border and are contained within some of the interchaos basins have an equivalent elevation to the surrounding nonfractured highlands.

and to the south by fractured plateaus of highland terrain (Figure 3). The largest (2 km wide) fractures run parallel to B5 and may be related to the formation and linear morphology of this basin. Unlike B1–B4, this basin is not located immediately adjacent to flood-grooved terrain.

[19] Basin 6 (B6) is composed of a series of irregular, interconnected topographic lows that mark the center of Iani Chaos (Figure 1). B6 is bounded by densely fractured cratered highland material and contains numerous isolated conical and plateau remnants. On average, the floor of B6 is

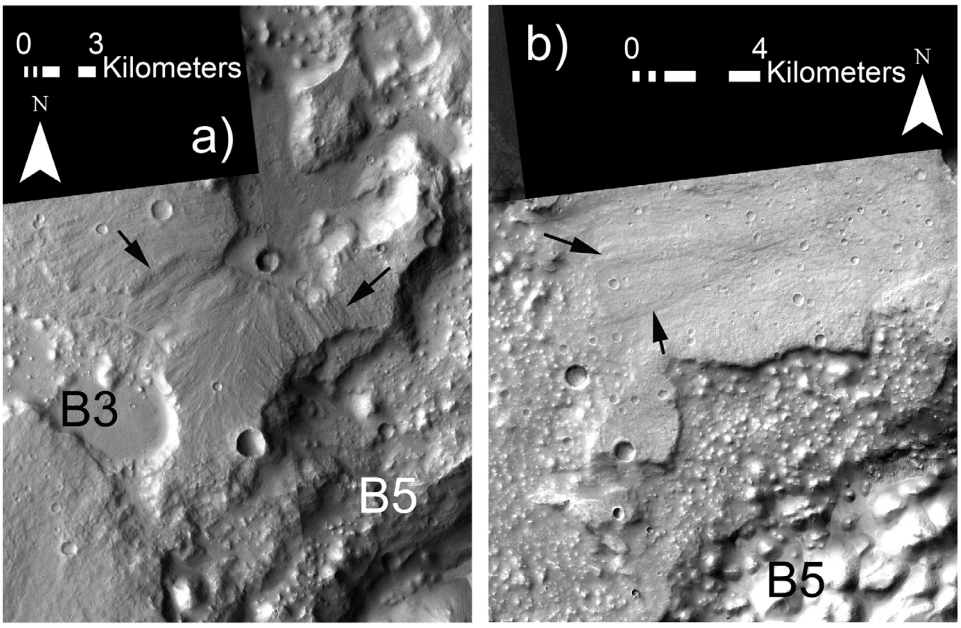

Figure 3. CTX mosaics displaying flood-grooved terrain (black arrows) on the northwest margin of Iani Chaos. The topography and groove orientations suggest eastward flow from small, shallow chaos basins toward Ares Vallis. (a) CTX images P04_002773_1784_XN_01S018W and P02_001995_1794_XN_00S018W illustrating grooved terrain east of B3. The northern rim of B5 truncates the grooves associated with this flooding event. (b) CTX images P15_006953_1767_XN_03S019W and B07_012504_1770_XN_03S020W displaying the grooved terrain to the west of B4. The southern margin of this flood surface is also crosscut by the younger basin B5.

significantly higher than B1, B2, and B5. This may in part be due to the presence of ILDs that cover a significant portion of the basin's floor (section 3.1.6). At its deepest point, B6 has a floor elevation of −4500 m, ~1.5 km below the surrounding highland terrain.

[20] Basin 7 (B7) comprises a series of interconnected basins in eastern Iani Chaos (Figure 1). B7 has a maximum depth of ~1.1 km. The lowest point of B7 corresponds with a circular topographic depression that may represent an ancient ~40 km wide impact crater. Within both the crater and the interconnected topographic depressions, B7 contains a number of densely fractured conical remnants, with discontinuous exposures of overlapping ILDs.

[21] Basin 8 (B8) represents the southernmost basin of Iani Chaos (Figure 1). B8 is a quasi-linear topographic depression with a general northeast strike. Similar to B5, several large fractures strike parallel to this basin. At its deepest point B8 is ~1.5 km deep (Figure 2e). There is no evidence within the basin, or adjacent to the basin, of flood eroded terrain (e.g., channels, streamlined remnants, and grooved terrain). The northern portion of B8 contains a thick, mounded outcrop of ILDs (section 3.1.6).

3.1.2. Basin Volume Estimates

[22] The topographic analysis suggests that the maximum elevation of the nonfractured highland terrain that bounds the eastern, western, and southern margins of Iani Chaos is comparable to the maximum elevation of many of the remnant fractured blocks that surround, and most importantly, are scattered at several locations within the centers of the eight interchaos basins (Figures 1 and 2). This observation suggests that the highland terrain was once continuous, with no major deviation in topography across the widths of the basins. Aside from B7, which may contain a large preexisting impact crater, the prominence and abundance of topographic highs within the basins negates the possibility that large topographic depressions (e.g., impact craters) were present at the locations of the eight basins before chaos formation. The interchaos depressions therefore represent regions of significant volume loss within the Martian crust. Below, we calculate the volume of the interchaos depressions to estimate the total volume loss of material in Iani Chaos and to compare these values to volume estimates of individual flood events within Ares Vallis.

[23] To calculate volume, we digitized the topographically irregular margins of each basin in ArcGIS, assigned an elevation value to each rim data point (3D point layer) from the HRSC DTM, and constructed a Triangulated Irregular Network (TIN) across the basin to represent the original, pre-chaos surface. The TIN was then converted to a 40 m gridded raster, from which the elevation values of the base HRSC DTM were subtracted to obtain the volume.

[24] Table 1 provides the results of the volume calculation for each basin. Figure 4 highlights the basin depth characteristics. It is noted that the HRSC DTM does not cover the entire extent of B5 and B8, but cuts each feature roughly in half. Furthermore, many of the basins are partially filled with sediments (ILDs) and/or mantles that superimpose the basin-floor topography. While our analysis of the ILDs

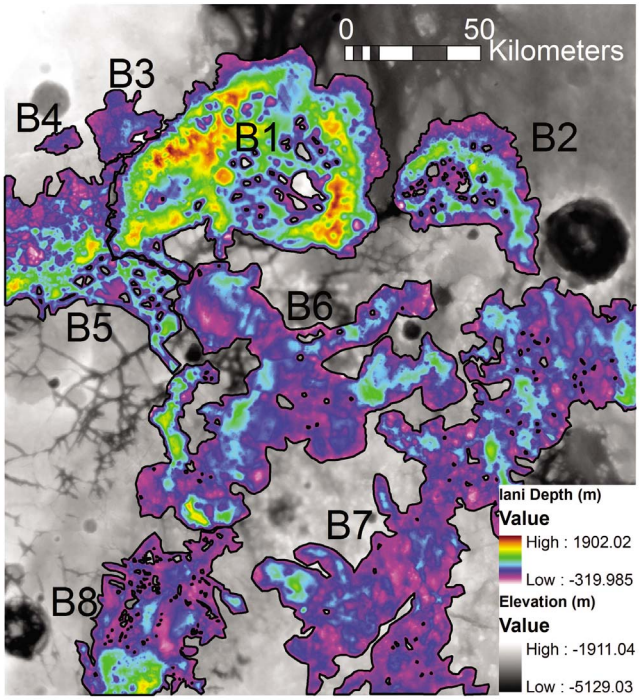

Figure 4. Depth map of the eight interchaos basins (B1–B8) displayed on the 40 m HRSC DTM. Basin volume (Table 1) was calculated by summing the calculated depths for each grid and multiplying that value by the grid area (1600 m^2). The total calculated volume of the Iani Chaos basins is 1.6×10^4 km^3.

(section 3.1.6) indicates that they may be relatively thin, we suggest that our estimates of volume loss from these basins are minimum values. The summed total volume of all the basins in Iani Chaos is 1.6×10^4 km^3.

3.1.3. Chaos Block Morphology

[25] The size and morphology of individual blocks and the density of block fields within chaotic terrains are likely directly correlative with the size, orientation, and spacing of extensional fractures [*Rodriguez et al.*, 2005a]. *Andrews-Hanna and Phillips* [2007] proposed that the regions of high block density in chaotic terrains were areas where hydrofracturing and water release generated numerous, closely spaced fractures, while *Rodriguez et al.* [2005a] proposed that the large plateau remnants, with low fracture density, represent regions of regional extension and limited subsidence.

[26] Figure 5 highlights the variety of block morphologies within Iani Chaos. In the highland marginal regions, large, kilometer-scale fracture systems create isolated plateaus that are up to ~60 km in diameter and have relief of up to ~2 km, measured from the floors of the bounding fractures (Figures 1 and 5a). These large plateaus contain exposures of layered bedrock and are often capped by a significantly thick (tens of meters) horizontally layered unit that is correlative across isolated plateaus and with the undisturbed highlands over tens of kilometers (Figure 5a).

[27] On the floors of the interchaos basins and superimposed on larger plateau remnants, are small conical mounds (Figures 5b and 5c). These features range in width from ~100 m to ~10 km and in height from tens of meters to ~1 km. In some regions, small conical mounds superimpose the fracture-bounded plateau remnants forming knobby plateaus (Figures 1 and 5c). This characteristic of overlapping block morphologies is restricted to the central and eastern regions of Iani Chaos (Figure 1). The maximum elevation of the mounds on the knobby plateaus is comparable to the elevation of the flat-topped fractured plateaus in western Iani Chaos and to the bordering, nonfractured highland terrain (Figure 1). The consistent defining characteristic of all the smaller conical forms is the lack of a resistant capping unit. The slopes of the mounds typically range between 20° and

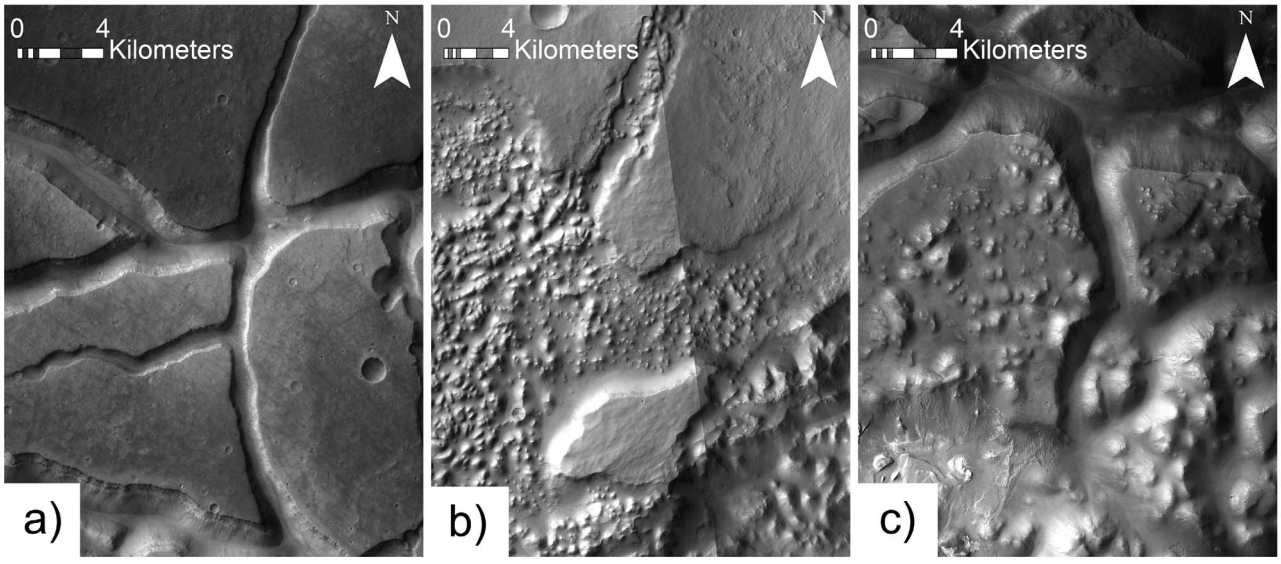

Figure 5. CTX images displaying different chaos block morphologies including (a) fractured plateaus (P15_006953_1767_XN_03S019W), (b) small conical mounds (P22_009603_1778_XN_02S018W and P04_002773_1784_XN_01S018W), and (c) plateaus superimposed by small conical mounds (knobby plateaus) (P02_001995_1794_XN_00S018W).

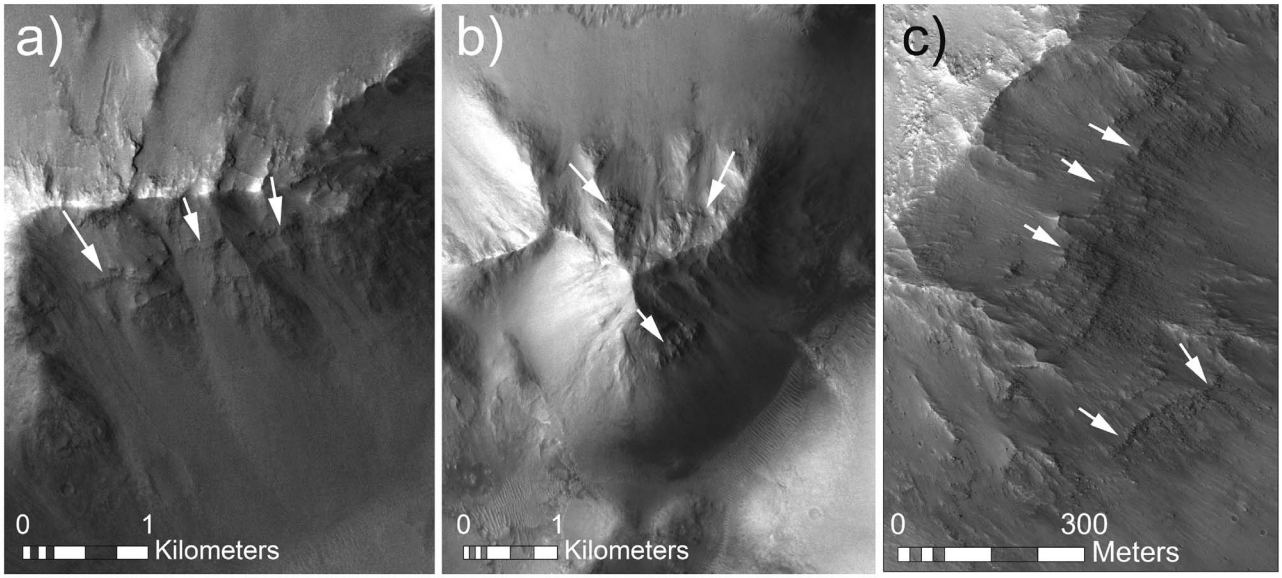

Figure 6. High-resolution images (CTX and High-Resolution Imaging Science Experiment, HiRISE) of small conical mounds within Iani Chaos. Subhorizontal to horizontal, meter-scale layering is visible along the flanks of mounds (white arrows). The pattern of layering and thickness of individual layers is generally consistent with layers exposed along the fractured highland plateaus and within the nonfractured highland terrain. (a) CTX image P13_006175_1774_XN_02S017W of layered stratigraphy in a small mound in southern B1. (b) CTX image P04_002562_1795_XN_00S017W of layers exposed in a conical mound in northern B1. (c) HiRISE image ESP_012728_1795_RED of layered, medium- to dark-toned layers in a mound in B1.

30°, near the angle of repose. Where the flanks of the mounds are exposed, an internal layered stratigraphy that is similar in scale and lateral continuity to the layers exposed within the fractured plateaus and the surrounding nonfractured highland terrain is visible (Figure 6).

[28] *Rodriguez et al.* [2005a] indicated from observational image analysis that subsidence and extensional fracturing of the highland terrain in Aureum Chaos only resulted in limited warping/tilting of the fractured highland plateaus. Here we quantify the tilt orientation and magnitude of the remnants of highland material in Iani Chaos, including both remnant plateau blocks and smaller conical mounds, to attempt to identify patterns in the warping/tilting of chaos blocks. By this method, the location, magnitude, and mechanism of subsidence and extensional warping of the highland terrain were constrained.

[29] For this analysis, we used ArcGIS and the HRSC DTM to measure both the slope angle and aspect (azimuth in degrees) of the upper surface of flat-topped plateaus in Iani Chaos to determine if the blocks underwent measurable rotation toward specific chaos depressions. We assume that the plateaus had an originally horizontal surface slope, controlled by the horizontal capping unit that is apparent on the surface of all the blocks measured for the aspect analysis (A–I) (Figures 5 and 7). For each plateau block, we identified any significant deviation from the magnitude and direction of the slopes as they compare to typical values of the surrounding, nonfractured highland terrain. This method assumes that secondary modification (erosion or deposition) of the upper surface has not smoothed the terrain on a regional scale, masking the primary tilt relationships of the blocks. This assumption is validated by (1) the lateral continuity of the horizontal capping unit across multiple blocks, (2) the vertical continuity in the horizontally layered strata in the blocks, and (3) our slope aspect map (Figure 7), which reveals steep interior plateau slopes (up to 50°) beneath the capping unit. These steep slopes indicate limited postformation erosional modification of the fractured margins of the plateaus. Regional surface slopes, measured across the nonfractured marginal highland terrain from individual MOLA transects, range between 0.01° and 3°, depending on the location and distance range (order of 100 km and 10 km, respectively) of the slope measurement.

[30] Figure 7 presents two example regional slope aspect maps for Iani Chaos derived from the HRSC DTM, regridded to 1 km for ease in visualization and aspect computation. For a selected plateau (A–I), we calculated the average aspect and the average magnitude of the slope. Specific blocks that are located proximal to interchaos basins B1, B5, and B8 were chosen to reveal if the blocks tilted or warped in response to basin formation. The results indicate that all plateaus have a consistent average surface slope of 2.5° to 4°, similar to the upper range of slopes calculated for the nonfractured highland terrain. Some measured plateaus that are proximal to the linear chaos basins B5 and B8 show a consistent slope aspect that suggests tilt toward the basins. As an example, the measured grids on plateau A provide a statistically consistent pattern of surface tilt to the northeast, toward the interchaos basin B5. The average slope of Block A is however low and similar to the upper bound slope of nonfractured highland terrain (~3°). The topographic profiles in Figures 2d and 2e also display basinward sloping surfaces for the plateaus

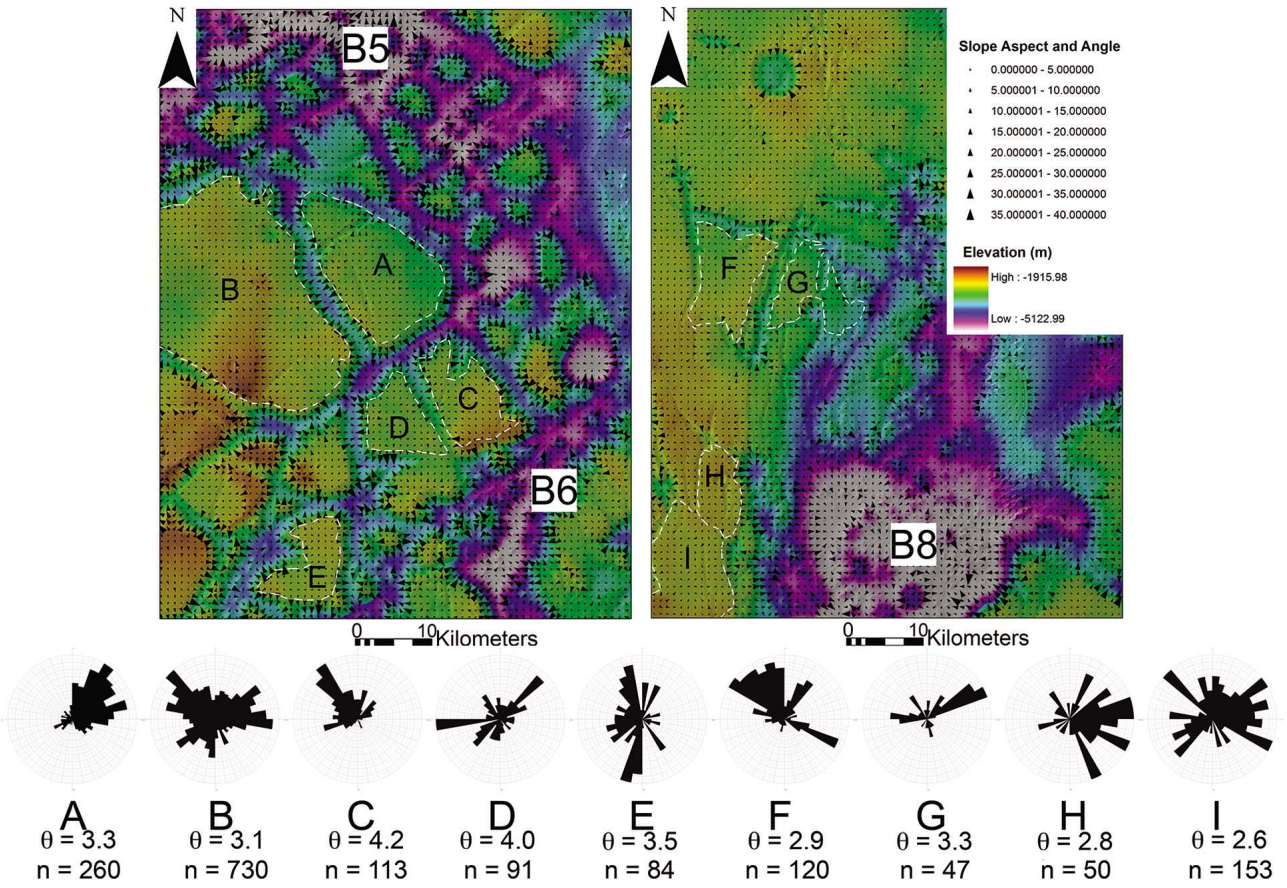

Figure 7. Slope aspect map displayed over the 40 m HRSC DTM. Each arrow illustrates the magnitude and direction of the average slope calculated from a 1 km size grid. Specific chaos blocks are highlighted to determine if the blocks show evidence for tilt toward the basins B5, B6, and B8. The results demonstrate that only some of the blocks that are most proximal to the basins show a consistent pattern in surface aspect. These blocks are tilted, with a surface slope (θ) of ~2.5°–4° toward the interiors of the basins. Blocks located distal to the basins show an apparent random surface aspect (n equals the number of measurements).

surrounding B5 and B8. This result may indicate limited subsidence (up to 300 m) beneath these plateaus and block tilt toward the interchaos basin. The majority of blocks distal to the collapse basins show an apparent random slope aspect.

[31] For smaller conical mounds that lack a smooth capping unit, the surface slope aspect cannot be calculated. Analysis of high-resolution CTX and HiRISE images revealed that the majority of small conical mounds have an internal layered stratigraphy that, upon initial examination, is similar in bedding thickness and dip to layered exposures in the surrounding highland terrain and remnant plateaus (Figures 6 and 8). Using the ArcGIS extension LayerTools [*Kneissl et al.*, 2010], we estimated the strike and dip of layers exposed within small conical mounds that are on the floors of interchaos basins. We hypothesized that the dip angles of the layers in these basin-floor mounds might show significant tilting of the blocks, caused by undermining and collapse. For comparison, dip estimates were repeated for layers exposed in the remnant plateaus.

[32] Layer contacts were identified at several locations on the fracture-bounded flanks of the plateau remnants. Layer contacts are sparse along the flanks of the smaller conical mounds. In many places, talus and/or mantling material obscure the flank exposures, particularly for the smallest (<1 km diameter) mounds. The results of the dip analysis for the small conical mounds are therefore limited, both owing to the lack of outcrops and the limited traceable extent of a single unit. The measurements for the mounds indicate dips of 2° to 9° (Figures 8a–8c), only slightly greater on average than the dip of the layers within the plateaus (1° to 3°) (Figure 8d). Furthermore, the measured layer dips for the plateaus are generally equal to the measured surface slopes. This validates that the surface slopes of the plateaus are reflective of the internal layered stratigraphy and that the aspect measurements taken from the upper surface of the plateaus reflect the tilt of the entire block. Consistent with the slope aspect results, from the LayerTools method we were unable to identify evidence for significant warping or tilting of the large plateau remnants. For the small mounds that occur within interchaos basins, the larger dip estimates for the exposed layers may be suggestive of block tilting during collapse, albeit limited to within 9° from horizontal.

3.1.4. Fracture Morphology

[33] Characteristic of all chaotic terrains, extension of the crust around interchaos basins has created complex polygonal fracture networks that extend into the undisturbed cratered

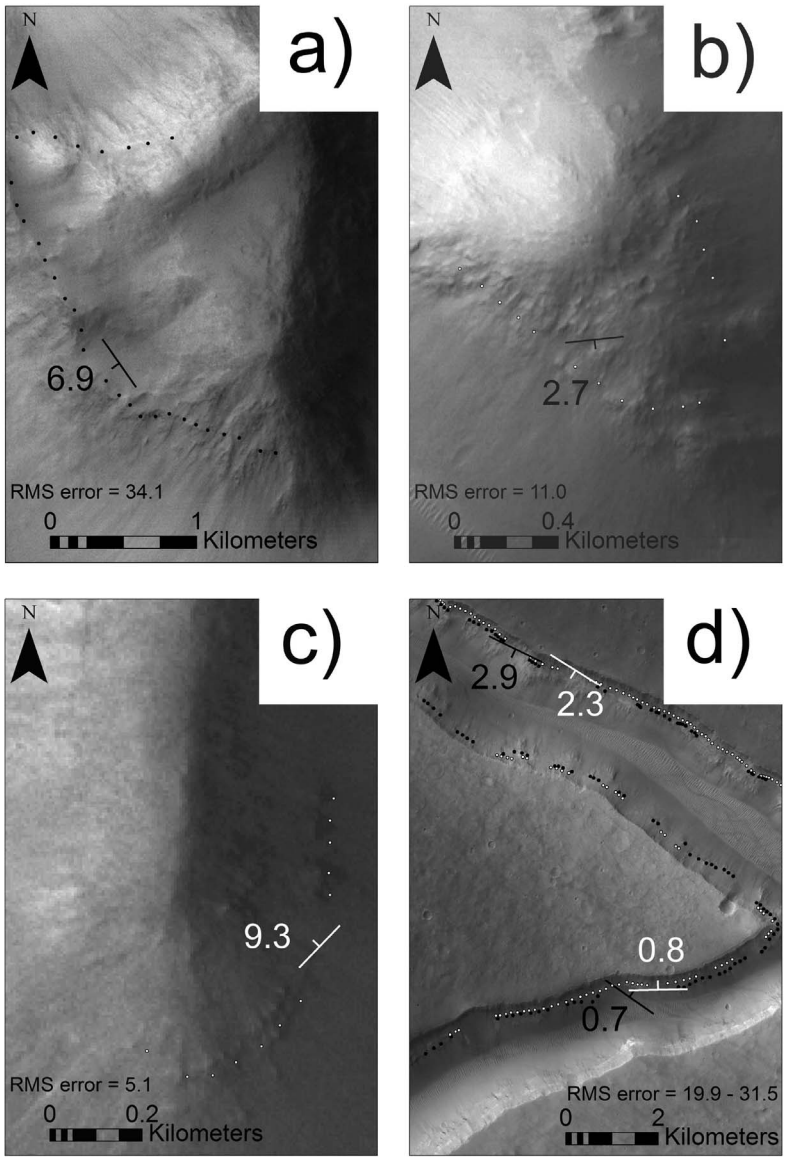

Figure 8. Select CTX images of chaos blocks and plateaus illustrating the strike and dip characteristics of the internal stratigraphy. (a) CTX image P02_001995_1794_XN_00S018W of shallow dipping (~2°) layers in a small mound in B1. (b) CTX image P22_009603_1778_XN_02S018W of a small conical mound in B6. Layers in this mound show a dip of ~7°. (c) CTX image P04_002773_1784_XN_01S018W showing layers within a small chaos mound in B6. Layers in this mound have a dip of ~9°. (d) CTX image P15_006953_1767_XN_03S019W of near-horizontal layers exposed on the flanks of a fractured plateau remnant of the highland terrain.

highlands. To the first order, the fractures in these networks exhibit an apparent random orientation. However, it has been proposed that global extensional stress fields may have facilitated local groundwater release at specific locations on Mars and influenced regional patterns in the formation of chaos basins [*Dohm et al.*, 2001; *Komatsu et al.*, 2004; *Lucchitta et al.*, 1994; *Rodriguez et al.*, 2005a]. Given this hypothesis, if the extensional fracturing associated with chaos formation is influenced by regional and global structural regimes, nonrandom patterns in the orientation of chaos fractures should be present.

[34] For this analysis we mapped the location and orientation of fractures within Iani Chaos to constrain the regional, paleostress field and to identify patterns relative to the interchaos basins. As for all chaotic terrains on Mars, fractures within Iani Chaos are extensional. Individual fractures have steep interior slopes (up to 50°), flat floors (filled with talus), and are characterized by a linear, curvilinear, or pit-chain planform morphology. Figure 9 illustrates examples of the digitized fractures overlain on the CTX mosaic. In total, approximately 15,000 fracture segments were measured across the CTX strips. The fractures range in width from a few

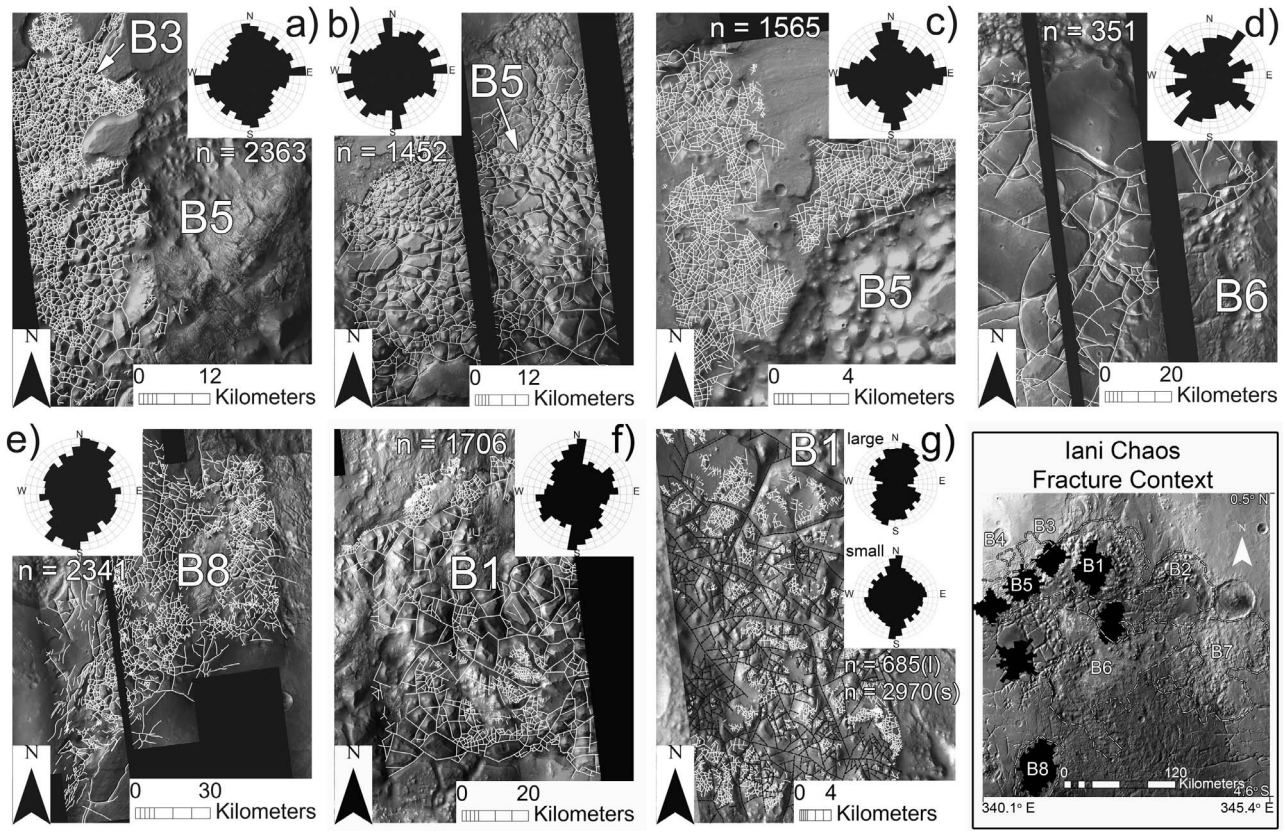

Figure 9. Montage of CTX mosaics in Iani Chaos displaying measured fracture patterns. Each map illustrates the digitized fractures and the orientations of the fractures on rose diagrams. The fracture orientations in Iani Chaos are not random. For several fracture zones, the fractures are aligned parallel to the orientation of linear chaos basins. This is particularly evident for Figures 9a–9c, 9e, and 9g (n equals the number of measurements).

meters to ~3 km, in depth from a few meters to ~2 km, and in spacing (measured across the largest width of a chaos block) from a few hundred meters to ~60 km. The general polygonal pattern of fracturing in Iani Chaos is independent of the scale and density of the fractures. However, in some regions, large fractures and pit chains follow parallel to the orientation of quasi-linear basins, such as for B5 and B8.

[35] From the fracture measurements, we have identified unique zones that have a consistent similarity in fracture density and scale in Iani Chaos. Importantly, these zones exhibit multiple overlapping, nonrandom fracture patterns and correspond with specific geomorphologic features, such as interchaos basins and smooth highland plateaus (Figure 9). Spatial associations have been identified that suggest a relationship between fracture morphology, orientation, and basin location. Specifically, most of the fracture zones, regardless of fracture scale, exhibit an average orientation that is consistent with the strike of associated basins (e.g., B5 and B8). The bordering nonfractured highland terrain grades into fractured plateaus of equal elevation that are surrounded by kilometer-scale fractures with a low fracture density. In this region, the fracture patterns also suggest a consistent alignment to nearby basins. In Zone 7 (Figure 9g), as well as in other regions of central, southern, and eastern Iani Chaos, large fracture systems crosscut densely fractured terrains. This relationship has resulted in a superposition of knobby terrain on large, isolated chaos plateaus. Several other examples of overlapping fracture systems are common and are obvious in the CTX imagery (Figure 10). The consistent relationship observed in the imagery is the crosscutting of smaller and shallower fracture sets by larger fracture systems.

3.1.5. Interchaos Flood Surfaces and Ares Vallis

[36] Figure 3 identifies interchaos flood surfaces along the northwest margin of Iani Chaos. They are identified by the occurrence of subparallel grooves that emanate directly from interchaos basins, including B3. We interpret these grooves to be the result of erosion by macroturbulence (e.g., roller vortices) in a flood [*Baker and Nummedal*, 1978] on the basis of their subparallel alignment to the local slope (directed toward Ares Vallis) and their morphologic similarity to previously described flood-grooved terrain throughout the circum-Chryse region [*Baker*, 1982; *Baker and Kochel*, 1979; *Carr*, 1979; *Komatsu and Baker*, 1997; *Nelson and Greeley*, 1999; *Scott and Tanaka*, 1986; *Tanaka et al.*, 2005; *Tanaka*, 1997].

[37] Figure 3a is a CTX image of the grooved terrain associated with interchaos basin B3. Figure 3b identifies the grooved terrain west of B4. The grooves are 100 m wide and are regularly spaced by 100 m to 200 m. For the grooves in the vicinity of B3, multiple surfaces with different groove orientations are observed. To the northeast of B3, grooves

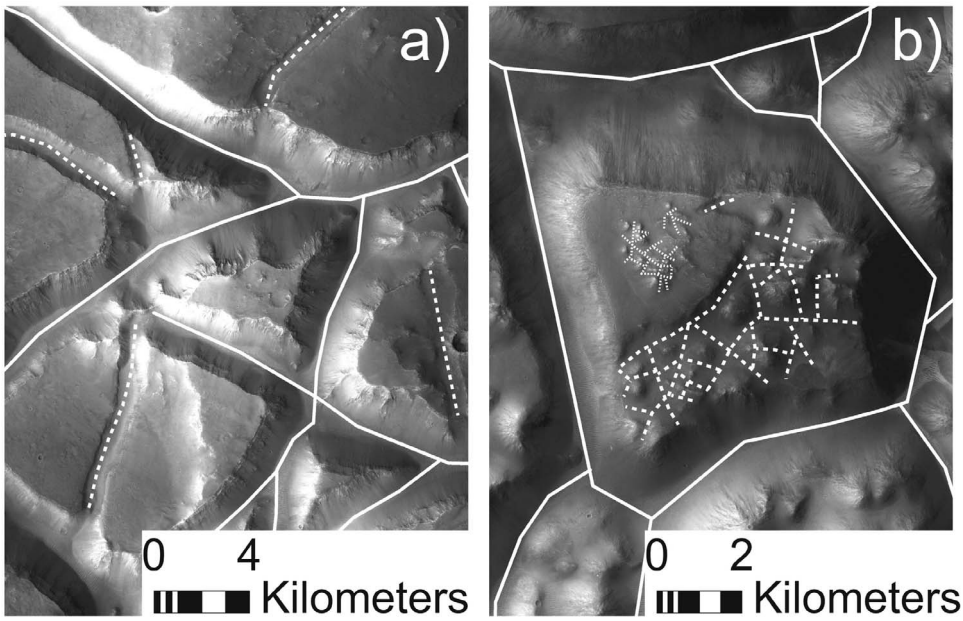

Figure 10. CTX images displaying overlapping patterns of fracture density and orientation in Iani Chaos: (a) CTX image P08_003973_1772_XN_02S019W of overlapping fracture patterns on large plateaus in western Iani Chaos and (b) CTX image P02_001995_1794_XN_00S018W of a dense set of fractures that are crosscut by larger fractures in central Iani Chaos.

with a northeast-southwest strike emanate from an oval, flat-floored depression. Further to the northeast, grooves with a perpendicular northwest-southeast strike are present. The southern margin of this groove set is truncated by the steep (up to 50°) northern scarp of B5 (Figures 2 and 3), suggesting that formation of the scarp wall (and thus B5) postdates formation of the grooves.

[38] The best defined flood eroded surfaces associated with Iani Chaos are the grooved terrains and flood channels of proximal Ares Vallis. These flood terrains emanate north from B1 and B2. Utilizing a 50 m HRSC DTM and impact crater chronology, *Warner et al.* [2009] mapped six distinct flood surfaces in proximal Ares Vallis. Here, using the improved 40 m HRSC DTM (Figure 11), we present a summary of this work, illustrating the location and elevation of these surfaces in the region proximal to Iani Chaos. Below, we describe the topographic relationships of northern Iani Chaos relative to the Ares Vallis flood terrain, with emphasis on the contact relationships between specific interchaos basins and grooved surfaces.

[39] The largest basin in Iani Chaos, B1, occurs at the head of the deepest and youngest (early Amazonian) (Table 2) [*Warner et al.*, 2009, 2010] outflow channel in Ares Vallis, Surface 6 (S6) (Figures 11a and 11b). At the northern margin of B1, S6 is 700 m higher than the floor of B1, with an average elevation of −4100 m. Along the east and west margins of B1, a topographically higher flood surface that bounds S6 is present. This surface, mapped as S5 is ~1 km higher than the floor of B1, with an average floor elevation of −3560 m (Figure 11a). Importantly, all grooves and smooth surfaces associated with S5 and S6 are truncated by the northern margin of B1 (Figures 11b and 11c). This suggests that the formation of this interchaos basin postdates the youngest, early Amazonian catastrophic flood events in Ares Vallis. Furthermore, there are no flood grooves, streamlined remnants, or channels within B1 that might be suggestive of post–basin formation catastrophic flooding.

[40] East of B1, B2 occurs at the head of the eastern branch of Ares Vallis, mapped as S4 by *Warner et al.* [2009] (Figures 11a and 11c). S4, carved in the early Hesperian, represents an early stage of catastrophic flood activity in Ares Vallis. The average elevation of S4, along the northern margin of B2 is −3310 m. The surface is perched ~900 m above the floor of B2. Bounding the western margin of B2, an ~8 km remnant strip of S5 separates the basin from B1 (Figure 11c). Importantly, the grooved terrains and channel remnants of both S4 and S5 are truncated by B2, suggesting that basin formation occurred after flooding on both surfaces. Furthermore, similar to B1, no channels, streamlined remnants, or grooved terrains were identified on the floor of B2.

[41] From CTX and HRSC image analysis, flood eroded terrain was not identified adjacent to the basins that occur in the interior of Iani Chaos, B5–B8. Rather, all preserved grooved terrains were identified along the northern margins of the chaos system. Flood eroded surfaces associated with the northwest highland margin of Iani Chaos (Figures 2 and 3) represent a previously undescribed source of flooding that may be directly related to events and features in the main channels of Ares Vallis. The groove orientations on these surfaces are consistent with water flow away from shallow chaos depressions and toward Ares Vallis (Figures 3 and 11a). From HRSC topography data, the average elevation of the distal extent (northeast edge) of the B3 grooved terrain is −2700 m (Figures 1 and 3). The grooved surface at this location is truncated by perpendicularly oriented flood channels that are associated with S5 and S6 (Figure 11a). Topographically, the B3 grooved terrain is perched ~1.5 km above S6. By comparison to other flood surfaces in Ares

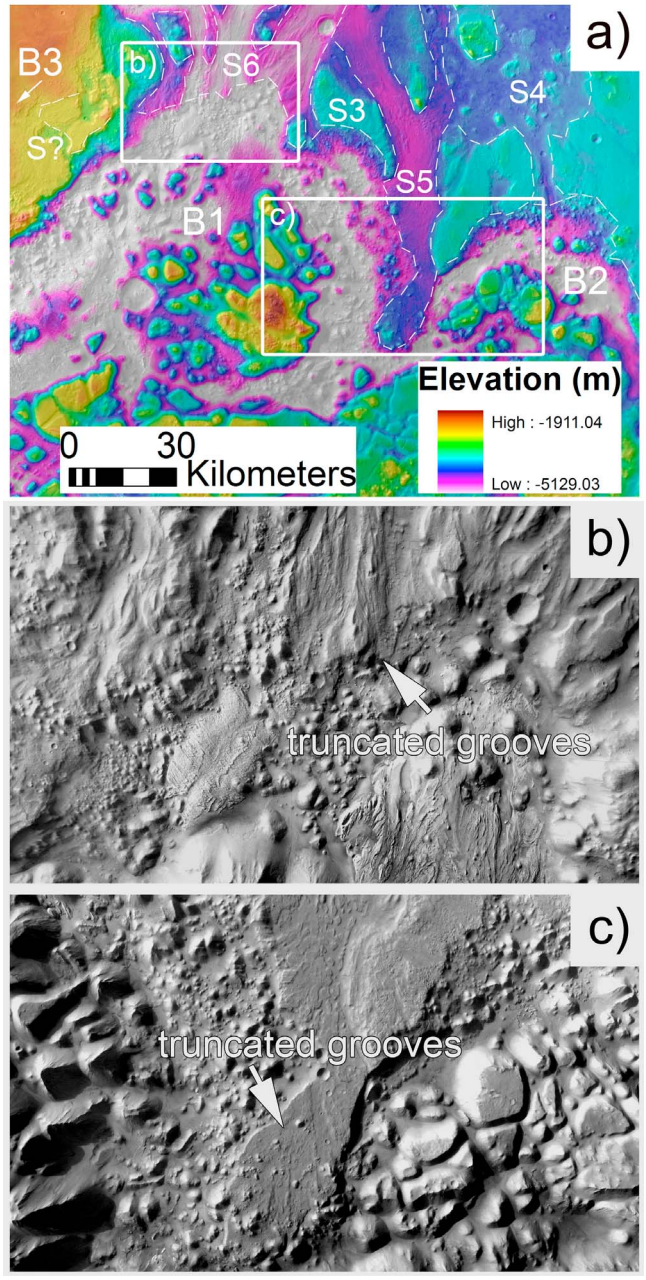

Figure 11. HRSC 40 m DTM and 15 m orthoimage displaying the topographic relationships between the proximal flood channels of Ares Vallis (S1-S6) [*Warner et al.*, 2009] and the northern inter-chaos basins of Iani Chaos (B1, B2). (a) The HRSC DTM highlights topographically distinct flood channels in Ares Vallis. These channels have a broad range of flood resurfacing ages, derived from impact crater statistics (Table 2), which suggest formation of S1–S4 in the early Hesperian and erosion of S5–S6 in the late Hesperian to early Amazonian. (b) The HRSC orthoimage (15 m) illustrates the relative relationship of B1 and S6. The flood grooves on S6 are truncated by the northern wall of B1, suggesting that B1 formed after erosion of S6. (c) The HRSC orthoimage highlights the relative relationship between B1 and B2 and S5. The interchaos basins truncate the grooved terrain of S5, leaving an older, elevated remnant flood surface.

Vallis, the elevation of these grooved terrains along the northwest margin of Iani Chaos is more consistent with the elevation of flooding associated with S2 or S3 (Figure 11 and Table 2) [*Warner et al.*, 2009] within proximal Ares Vallis.

3.1.6. ILDs and Mantling Deposits

[42] Interior layered deposits (ILDs) in Iani Chaos are identified by discrete stacks of meter-scale, subhorizontally layered, light- to medium-toned materials that superimpose chaos blocks and fractures. Importantly, the ILDs are not always associated with the topographically lowest points in Iani Chaos, but occur both within the interchaos basins and along their elevated margins. The stacks range in relief from 60 m to as high as 800 m. It is from these units that mineral signatures associated with sulfate and crystalline hematite have been detected from visible-light, near-infrared, and thermal infrared spectral data [*Dobrea et al.*, 2008; *Gendrin et al.*, 2005; *Glotch and Rogers*, 2007].

[43] For our analysis, we have identified laterally extensive stacks of ILDs in six unique locations (I1–I6) (Figure 12). We have also identified dozens of isolated layered remnants throughout Iani Chaos. In the analysis below we present a description of the spatial and morphologic characteristics of the six deposits as they relate to geomorphic features of Iani Chaos and Ares Vallis to attempt to understand the relative chronology of the ILDs and their possible mechanism of formation. A mineralogic assessment and detailed stratigraphic analysis is beyond the scope of this paper. For recent discussions on these topics, see the work of *Dobrea et al.* [2008] and *Glotch and Rogers* [2007].

[44] Initial inspection of the ILDs in Iani Chaos by *Dobrea et al.* [2008], *Glotch and Rogers* [2007], and *Gendrin et al.* [2005] suggested that the ILDs are associated with the lowest topographic points in the chaos system. From the HRSC data, this assessment holds true only for one ILD exposure within B1 (I1). Within B1, three discrete ILDs are present (I1–I3).

[45] I1 is a ~200 m thick, 6 km diameter raised mound of layered material located along the northern interior rim of B1, adjacent to grooved terrain of Ares Vallis (Figures 12 and 13a). Characteristic of all ILDs analyzed here, I1 overlies the knobby surface on the floors of the interchaos basins (Figure 13a). Fractured knobby terrains that can be traced up to the margins of I1 disappear and are superimposed by the layered deposits. This indicates that chaos-related fracturing and block formation in B1 predates formation of I1. By comparative relative chronology as discussed in section 3.1.5, I1 therefore must also postdate the last catastrophic flooding event (S6) within Ares Vallis. The surface of I1 has a maximum summit elevation of −4360 m (Figure 14a) and exhibits well-defined subparallel grooves. The northwest-southeast strike of the grooves on I1 is oblique to the north-south strike of flood-carved grooves within the adjacent bedrock flood channel, S6 (Figure 11). The basin proximal flood surface of S6 is ~310 m higher than the highest surface of the I1 (Figure 14a).

[46] Located 10 km east of I1, I2 (Figures 12 and 13b) is an elongate surface of exposed ILDs. With a maximum surface elevation of −3700 m, I2 perches ~350 m above the topographically lowest Ares Vallis flood channel, S6 (Figure 14b). I2 exhibits north-south striking surface grooves. From the lowest point in B1, I2 has ~800 m of relief. However, this thickness estimate may not be accurate if the ILD is present

Table 2. Impact Crater Statistics for Iani Chaos and Ares Vallis[a]

Surfaces	Area (km^2)	Counts	N(0.05)	N(0.1)	N(0.5)	N(1)	N(5)	Model Age From Fit (Ga)	Relative Age
This Study (Iani Chaos)									
Fractured plateaus	30474	23149	NA	7.6×10^5	2.0×10^4	4.7×10^3	6.9×10^2	3.08[b] (+0.07, −0.10); 3.90 (+0.03, −0.04)	LH[b,c], EA[b,d]; MN[c], MN[d]
Floor-fractured crater	693	899	NA	1.3×10^6	1.6×10^4	1.4×10^3	NA	2.87 (+0.33, −0.56)	LH[c], EA[d]
Grooved terrain (west)	74	156	NA	2.1×10^6	1.4×10^4	NA	NA	2.87 (+0.24, −0.34)	LH[c], EA[d]
ILD north (I1, I2, I3)	882	170	1.9×10^5	5.3×10^4	1.1×10^3	NA	NA	0.02 (+0.003, −0.003)	LA[c], LA[d]
ILD central (I4)	3153	436	1.4×10^5	4.3×10^4	9.5×10^2	NA	NA	0.10 (+0.03, −0.03)	LA[c], LA[d]
ILD east (I5)	62	24	3.9×10^5	8.1×10^4	NA	NA	NA	0.04 (+0.01, −0.01)	LA[c], LA[d]
ILD south (I6)	408	44	1.1×10^5	4.2×10^4	4.9×10^3	NA	NA	0.02 (+0.005, −0.005)	LA[c], LA[d]
Mantling unit	333	399	NA	1.2×10^6	9.0×10^3	NA	NA	0.71 (+0.05, −0.05)	MA[c], MA[d]
From Warner et al. [2009] (Proximal Ares Vallis)									
S1	1164	1189	NA	1.0×10^6	1.7×10^4	3.4×10^3	NA	3.60 (+0.07, −0.14)	LN[c], EH[d]
S2	525	59	NA	NA	1.9×10^4	3.8×10^3	NA	3.62 (+0.09, −0.27)	LN[c], EH[d]
S4	2243	1795	NA	8.0×10^5	1.3×10^4	3.6×10^3	NA	3.62 (+0.08, −0.18)	LN[c], EH[d]
S5	1149	115	NA	NA	9.6×10^3	1.7×10^3	NA	2.53 (+0.81, −1.80)	EA[c], EA[d]
S6	5735	3078	NA	5.4×10^5	9.9×10^3	1.7×10^3	NA	2.86 (+0.39, −0.76)	LH[c], EA[d]
From Warner et al. [2010] (Proximal-Distal Ares Vallis)									
S6	21720	13781	NA	6.3×10^5	1.4×10^4	2.5×10^3	NA	2.54[b] (+0.13, −0.13), 3.73 (+0.04, −0.05)	EA[b,c], EA[b,d]; LN[c], EH[d]

[a]Statistics for each surface are displayed as N(X), where N is the cumulative number of craters counted on a surface per 10^6 km^2 and X is the given diameter range in kilometers. Absolute model ages are derived from crater production and chronology functions presented by *Ivanov* [2001] and *Hartmann and Neukum* [2001]. NA, data not available; E, early; M, middle; L, late; N, Noachian; H, Hesperian; A, Amazonian.
[b]Resurfacing correction.
[c]Hartmann age system.
[d]Neukum age system.

only as a thin veneer on an underlying topographic high. Three-dimensional HRSC perspective views reveal onlapping characteristics between layers of I2 and a nonlayered conical mound (layers in the mound may be obscured by talus) (Figure 15a).

[47] I3 is a 45 km long, 18 km wide mounded ILD exposure located immediately within the western margin of B1 (Figures 12 and 13c). Figure 14c provides a northwest-southeast topographic profile taken perpendicular to the strike of the mound. The summit elevation of I3 is −3630 m, approximately 420 m higher than S6 in Ares Vallis, and ~300 m lower than S4. Measured from the bottom of the mound to the summit, the mound has ~700 m of relief. However, perspective views of I3 reveal onlapping relationships between conical mounds of remnant highland material and the layered deposits (Figure 15b). Similar to I2, this suggests that I3 may be thinner than its total relief implies as it may drape preexisting elevated topography. The upper surface of the ILD mound is grooved, showing a northwest-southeast groove orientation that is oblique to grooves on I2, but consistent with the groove orientation on I1. However, local variations in groove orientation are obvious (Figure 13c), particularly around the conical mounds and margins of the deposit where grooves are perpendicular or oblique to the general northwest pattern.

[48] I4, located near the center of Iani Chaos (Figures 12 and 13d), represents an aerially extensive ILD that exhibits obvious meter-scale horizontally layered stratigraphy of alternating light and medium-toned material. The average elevation, taken across the surface of I4, is −3400 m (Figure 14d), approximately 650 m higher than the chaos-proximal elevation of S6. Similar to other ILDs in Iani Chaos, fractures truncate abruptly against I4. This also suggests that deposition of the layered materials postdates fracturing and mound formation. Unique to the previously described ILDs, I4 shows no evidence for surface grooving. Rather, the deposit is either laterally continuous, with a smooth surface, or has been degraded into small remnant layered mounds

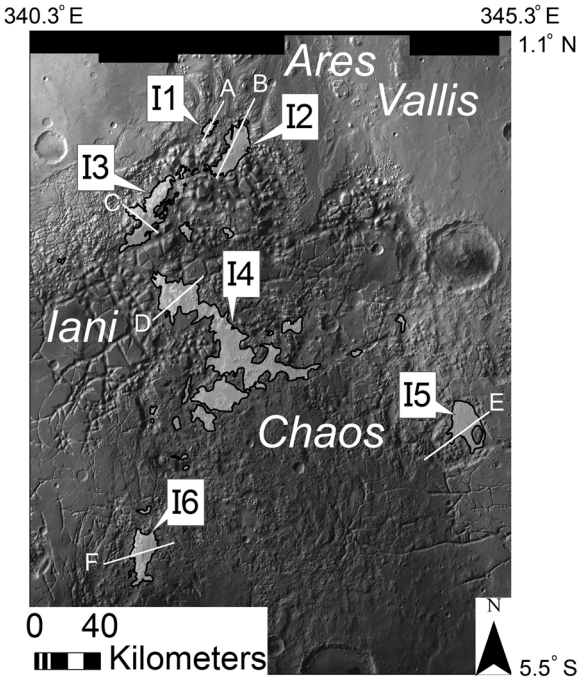

Figure 12. HRSC orthomosaic (15 m) of Iani Chaos displaying the locations of the six interior layered deposits (I1–I6) discussed in this analysis. Transects A–F are also drawn on the image. The topographic profiles from these transects are displayed in Figure 14.

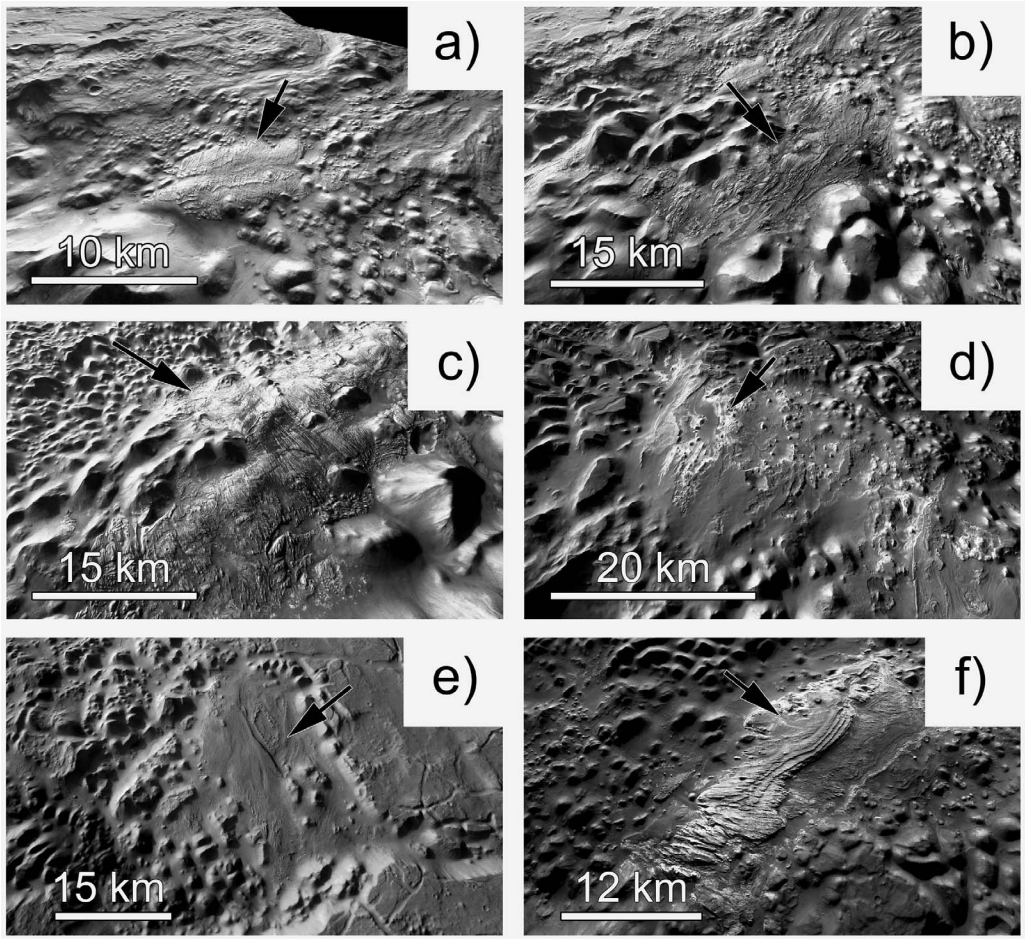

Figure 13. Perspective views from the 40 m HRSC DTM overlain by the 15 m orthoimage of the six ILD deposits (black arrows) in Iani Chaos. The ILDs occur within and along the margins of the interchaos basins. Each ILD consists of subhorizontal stacks of intermediate- to light-toned layered material. The surfaces of the ILDs are characterized by subparallel grooves (aside from I4), the pattern of which suggests erosion by wind. Figures 13a–13f correspond to ILDs I1–I6, respectively. The scale bars are generally consistent with objects in the foreground of the image.

(Figure 13d). A 20 m thick, medium-toned mantling unit occurs on top of I4 (Figure 16). This mantling unit drapes not only the lighter toned deposits of I4, but the surrounding conical chaos blocks and highland plateaus. We have identified this medium-toned mantling unit throughout the entire aerial extent of Iani Chaos, including regions of the highland terrain beyond the study area. The deposit is cliff forming where it is being degraded (Figure 16a), occurs at varying elevations (Figure 16b), and in some cases completely obscures the flank stratigraphy of small chaos mounds.

[49] In eastern Iani Chaos, I5 is composed of a series of isolated ILD exposures, largely centered within specific topographic lows in B7 (Figures 12 and 13e). There are two primary deposits that occur within northern and southern B7. The northern deposit is a 4 km wide ILD exposure that is characterized by an etched surface with northwest-southeast oriented grooves. The maximum surface elevation of this feature is −3750 m, with a total relief of ~70 m, measured from the basin floor to the top of the deposit. Meter-scale horizontal layering is visible along the southeast margin of the exposure. The southern deposit in B7 superimposes the interior of a 40 km wide, fractured circular basin that may represent a prechaos impact crater (Figure 13e). The maximum elevation of this deposit is −3390 m and has a total relief of ~250 m.

[50] Finally, I6, located on the floor of B8 in southern Iani Chaos, is a thick stack of westward dipping layered light-toned materials with a maximum summit elevation of −3130 m (Figures 12, 13f, and 14f). Figure 14f displays a topographic cross section of I6 and reveals ~700 m of vertical relief. HRSC perspective views (Figure 15c) of I6 reveal a thick vertical stack of subhorizontally layered medium- to light-toned layered units. At the base of the exposure, medium-toned layered deposits drape conical mounds that are likely chaos blocks/remnants of fractured highland terrain. This observation suggests that I6 postdates chaos formation.

3.2. Impact Crater Chronology

3.2.1. Prechaos Highland Terrain

[51] Impact crater statistics were obtained from the surface of the fractured plateau remnants of the cratered highland

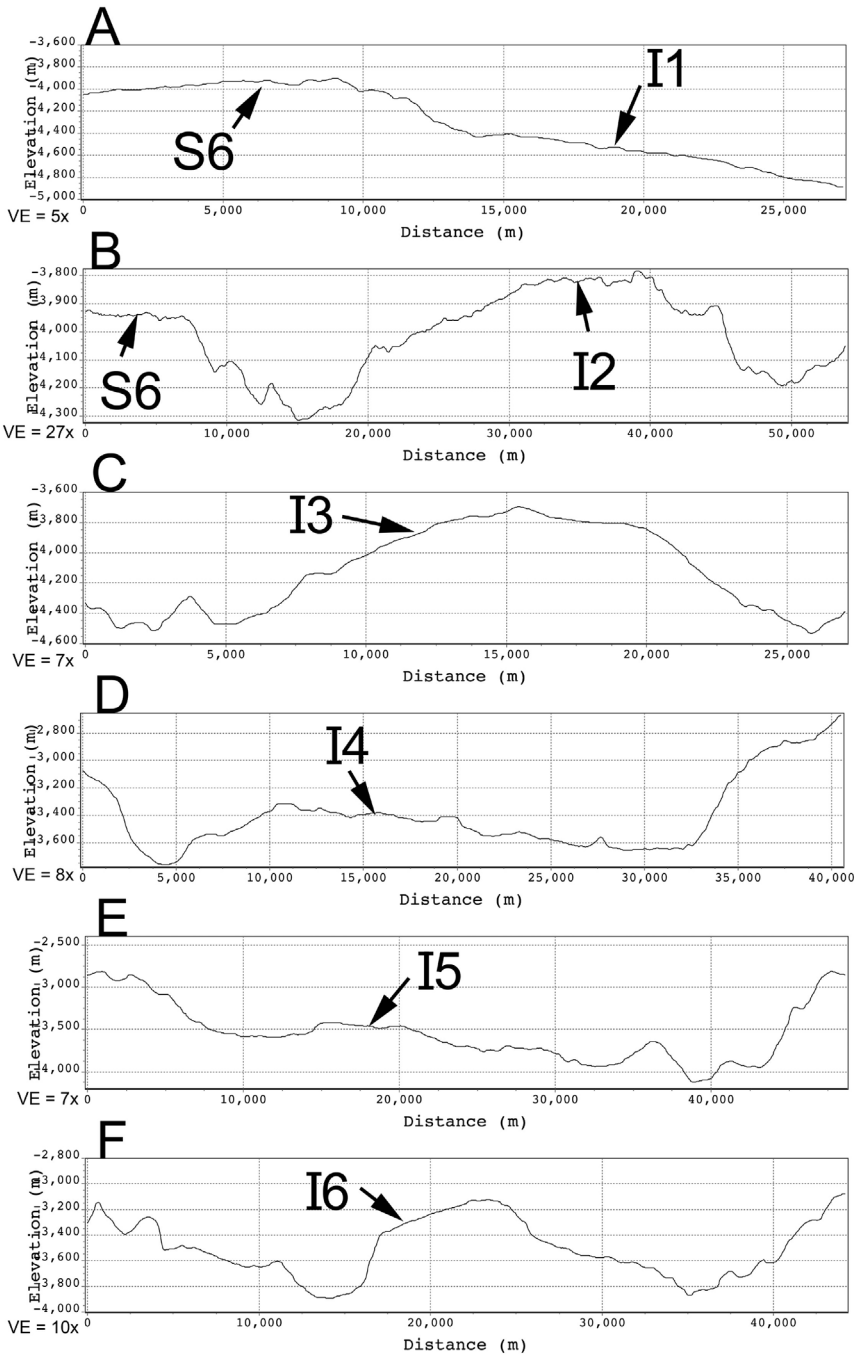

Figure 14. Topographic profiles of the ILDs in Iani Chaos, corresponding with transects across the ILDs presented in Figure 12. Each ILD consists of a mound of layered materials ranging from 60 to 800 m in height, measured from the base of the associated interchaos basin. Transect B highlights the topographic relationship between I2 and the topographically lowest flood surface of Ares Vallis, S6. Here, the upper surface of I2 is ~350 m higher than the nearby flood surface.

terrain, located along the western and eastern boundaries of Iani Chaos (Figure 17). The surfaces of the remnant plateaus are characterized by a relatively smooth landscape that is morphologically and topographically consistent with the highland plains that surround Iani Chaos. *Tanaka et al.* [2005] mapped the highland terrain in this region as part of the early to middle Noachian age Libya Montes unit from craters with $D > 5$ km.

[52] Table 2 provides the crater statistics for all surfaces in this study, including the Ares Vallis flood surfaces from *Warner et al.* [2009, 2010] for comparison. For the remnant plateaus, over 23,000 impact craters with $D > 100$ m were counted from the CTX mosaic over an area of ~30,000 km^2.

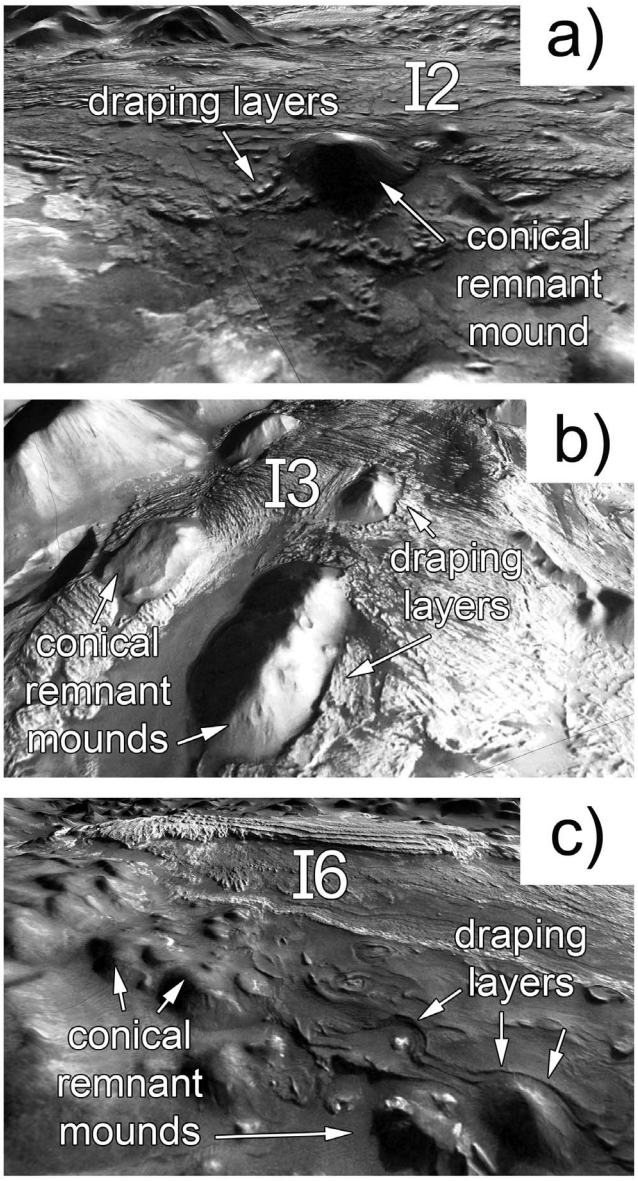

Figure 15. Perspective views of ILDs in Iani Chaos from the HRSC DTM: (a) layered materials within I2 drape a conical mound on the floor of B1, (b) light-toned layered materials within I3 embay against conical mounds within B5, and (c) layered materials within I6 cover small conical features on the floor of B8. These observations suggest that the ILDs are younger than the interchaos basins that contain the small conical mounds.

Figure 18a illustrates the cumulative frequency histogram for counts taken from the plateaus. For craters with D > 2.6 km, the data closely follow the 3.9 Ga isochron indicating a model formation age of middle to late Noachian (Table 2), consistent with the findings by *Tanaka et al.* [2005]. However, our data reveal a previously undescribed major deviation from the 3.9 Ga isochron for D < 2.6 km. The slope of the cumulative frequency curve between D = 700 m to 2.6 km declines gradually until a fit is reestablished at 3.0 Ga for D = 200 m to 700 m, indicating a late Hesperian resurfacing event. At diameters less than 200 m, the general rollover in the data may be the result of either (1) preferential destruction of the smallest crater population by dust infill or other erosive/burial processes or (2) human error in counting the smallest, most abundant crater population.

3.2.2. Crater Modification and Fracture Age

[53] The largest diameter craters (D > 8 km) within Iani Chaos show varying states of preservation, with some craters that have distinct ejecta blankets and rims and some that lack ejecta, have heavily modified rims, and contain significant infill. The layered infill material in some modified impact basins exhibit networks of polygonal fractures that sometimes form chaos-block morphology and often have interior rim moats that are typical of other floor-fractured craters (FFC) on Mars [*Rodriguez et al.*, 2005a; *Sato et al.*, 2010]. FFCs on Mars are preferentially located near chaotic terrains and outflow channels, including Iani Chaos and Ares Vallis, and are therefore likely related to the evacuation of water, subsurface volume loss, and extensional fracturing at these locations.

[54] Figure 19 identifies one particular FFC, located along the southern margin of Iani Chaos at 5.5°S, 343.5°E. The crosscutting relationship of the crater floor materials to the fractures indicates that extensional fracturing of the FFC occurred after the floor materials were emplaced. Figure 18b provides the cumulative frequency histogram of craters with D > 100 m on the surface of the floor material. The data (Table 2) indicate a best fit to the 2.9 Ga isochron for the floor of material at D = 400 m to 1 km. At D < 400 m the curve deviates significantly from the isochron indicating preferential removal of the smaller craters. It should be noted that the model age error for the floor of this crater (+0.3, −0.6 Ga) indicates substantial variability in the potential age of formation (Hesperian to early Amazonian). This error is due to the small area of the analysis and limited number of craters (25) with diameters between 400 m and 1 km, from which the fit was constructed. From this data set, extensional fracturing of the floor material within the crater can be constrained to a time during or after the Hesperian. By association with adjacent fracture systems in Iani Chaos, this loosely constrains the timing of fracturing in Iani Chaos to this time period.

3.2.3. Chronology of Associated Flood Surfaces

[55] High-resolution image analysis reveals interchaos channel floors that are defined by regularly spaced longitudinal grooves. Two grooved floor remnants were identified within Iani Chaos, proximal to the shallow chaos basins on the northwest margin of Iani Chaos (B3 and B4) (Figures 2 and 3). Inferred flow direction from groove orientation suggests that flow occurred to the east, from discrete, shallow chaos depressions, toward proximal channels of Ares Vallis. The areas of these surfaces are small and the cumulative crater frequency histograms reveal significant errors (maximum error of +/−300 Ma) in the model ages (Figure 18c). However, the ages are consistent with the general Hesperian to early Amazonian timing of circum-Chryse floods [*Marchenko et al.*, 1998; *Nelson and Greeley*, 1999; *Rotto and Tanaka*, 1995; *Tanaka and Skinner*, 2004; *Warner et al.*, 2009].

[56] From the topography, the B3 and B4 grooved terrains are not likely related to the topographically lowest and youngest flood events in Ares Vallis, S5–S6 (Figure 11). For these surfaces to have formed as the result of a chronologi-

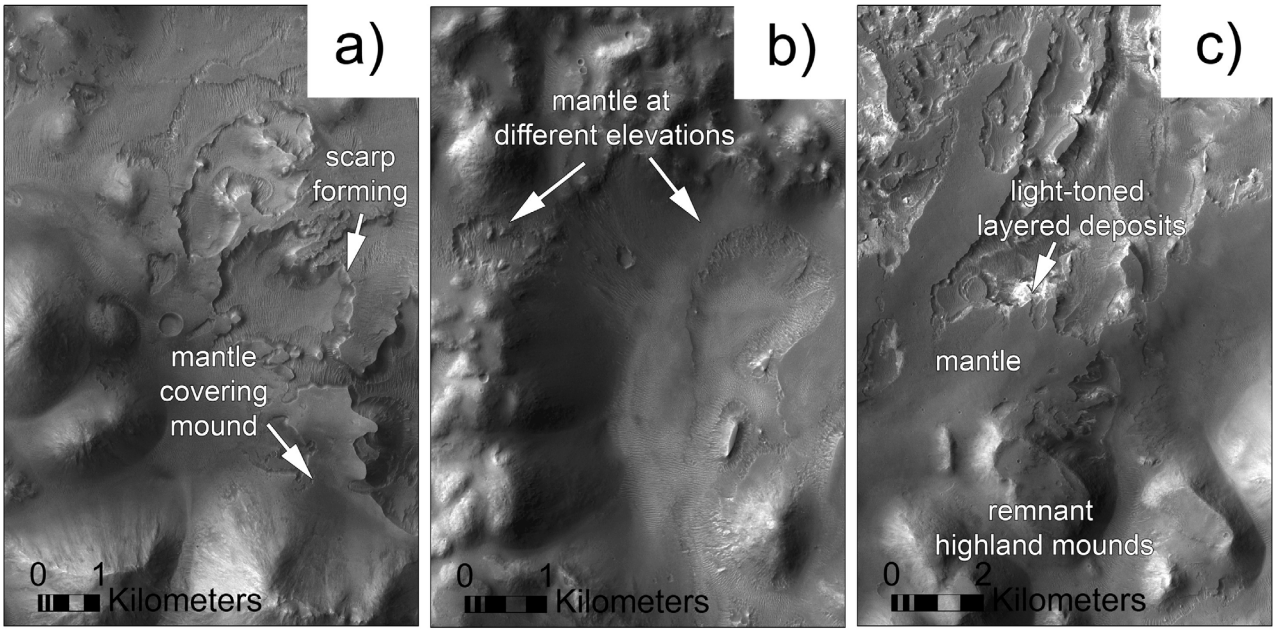

Figure 16. CTX images highlighting example locations of the regionally extensive mantling unit in Iani Chaos. (a) CTX image P02_001995_1794_XN_00S018W showing degradation of the mantling unit. In many places in Iani Chaos the mantle is scarp forming, suggesting that the material is well indurated. (b) CTX image P22_009603_1778_XN_02S018W illustrating the draping characteristic of the mantling unit. In this image, the mantle occurs both at the base and on the upper surface of a 400 m tall scarp. (c) CTX image P02_001995_1794_00S018W displaying the medium-toned mantling unit in central Iani Chaos. Here, within B6, the mantling unit overlies small conical mounds and light-toned ILDs associated with I4.

cally synchronous event, flooding from B3 and B4 would have flowed over a substantial elevation drop of ~1 km over a short distance of only 30 km. There is however no evidence for grooves, channels, or cataracts between these two surfaces that would suggest continuous, time-synchronous flow over a large gradient. Rather, it is more likely that these topographically high interchaos flood surfaces are related to the older, topographically higher, early Hesperian age flooding events in Ares Vallis, including S2–S4 (Table 2). We exclude S1 from *Warner et al.* [2009] as a related surface because it is topographically higher at its downstream origin than the B3 and B4 grooved terrain.

3.2.4. Chronology of ILDs

[57] Table 2 presents the crater count statistics for the most regionally extensive ILDs in Iani Chaos. These include the northern ILD exposures in B1 (I1–I3) (Figure 18d), the central exposures within B6 (I4) (Figure 18e), the eastern exposures in B7 (I5) (Figure 18f), and the southern exposures in B8 (I6) (Figure 18g). Impact craters on these surfaces are poorly preserved relative to craters on the highland plateaus and basin floors (Figure 20). These features lack ejecta, are commonly infilled with lower albedo material, and have subdued rims that are superimposed by subparallel grooves. This morphology indicates that the ILDs do not easily preserve impact craters, and thus suggests that any model age derived from these features will not be representative of their true formation age.

[58] For the northern ILD surfaces (Figure 18d), the crater cumulative frequency histogram indicates a steady decline in slope for all diameter bins beneath D = 1.3 km (the largest crater on the northern ILD surfaces = 1.3 km). A fit to the entire diameter range provides a model age of ~25 Ma (+3.2, −3.3), or late Amazonian relative age. For the central deposits, which have the largest aerial extent in Iani Chaos (Table 2), a fit from D = 200 m – 500 m suggests a late Amazonian model age of 100 Ma (+25, −26) (Figure 18e). A sharp decline in the cumulative frequency curve occurs on this surface at D < 200 m, indicating preferential removal of the smallest diameter craters. For the eastern deposit, the crater statistics indicate a fit to the late Amazonian, 44 Ma (+13, −13) isochron for craters with D = 50 m – 100 m (Figure 18f). Finally, for the series of ILDs in southern Iani Chaos, a good fit to the 22 Ma (+5.3, −5.5) isochron is obvious for craters with D < 200 m, with few craters available at larger diameters (Figure 18g). In summary, all ILDs in Iani Chaos have a late Amazonian crater retention age.

4. Discussion

4.1. Fracture-Controlled Collapse Origin of Iani Chaos

[59] The fracture analysis (Figure 9) and topography data (Figure 2) provide important clues to the origin of Iani Chaos. Extensional fractures associated with chaos formation, on a local (within individual basins) and regional scale (across Iani Chaos), are not randomly oriented. Furthermore, the observed consistency in the alignment of quasi-linear basins (B5, B8) (Figure 1) and fracture systems indicates a genetic correlation between basin formation processes and extensional fracturing

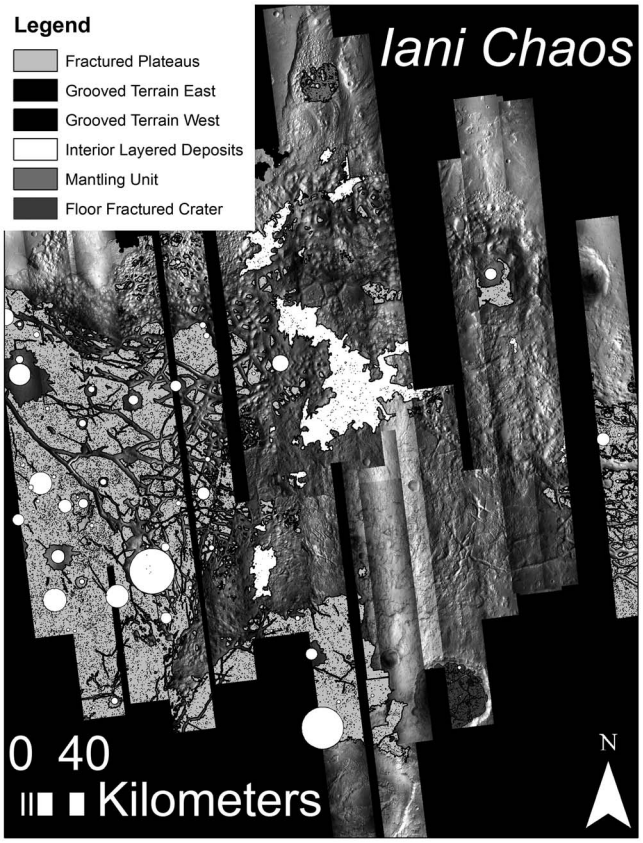

Figure 17. CTX mosaic displaying the impact crater counts (D > 100 m, except ILDs) for mapped surfaces in Iani Chaos, including the fractured plateaus, ILDs (D > 50 m), interchaos grooved terrain, mantling unit, and crater floor infill for a single floor-fractured crater in southern Iani Chaos. The statistics from these counts are presented in Table 2. The cumulative crater frequency histograms are presented in Figure 18.

of the crust. From the topographic and stratigraphic observations that indicate a previously continuous highland surface across the interchaos basins (Figures 2 and 5a), we suggest that the most likely mechanism for generating polygonal networks of extensional fractures in association with deep basins is by collapse-induced extension of the crust, a result of undermining of the subsurface (volume loss). Volume loss from depth (1 km to 2 km) and collapse likely resulted in regional extension and formation of the kilometer-scale (depth, width, and length) fracture sets.

[60] The regional fracture analysis (Figure 9) revealed a consistent variation in the orientation of fractures between northern and southern Iani Chaos. For northern Iani Chaos, we identified a dominant ENE-WSW directed fracture system that is aligned parallel to the general strike of B5 and suggests maximum NNW-SSE directed extensional stress. In the south, the dominant NNE-SSW orientation of fractures indicates a WNW-ESE component of extension. These patterns, and their relationship to the orientations of interchaos basins, are best explained if some preexisting condition of extensional stress in the region influenced not only the location of collapse events but also the alignments of the resultant extensional fractures. Furthermore, multiple directional components of maximum extension were identified for specific regions and may indicate multiple overlapping, preexisting extensional patterns and/or multiple basin formation events (Figures 9 and 10). For the large semicircular basins (B1, B2, B6), fracture control is less obvious, however, these features occur at the locus of intersection of the quasi-linear basins B5 and B8 and may thus represent a prechaos condition of enhanced crustal weakness.

[61] The slope aspect data provide further important clues to the nature of collapse in Iani Chaos (Figure 7). As postulated by *Rodriguez et al.* [2005a], we hypothesized that collapse-induced extension of the highland terrain within Iani Chaos may have caused warping/tilting of the basin-bounding highland crust. However, the slope aspect analysis, topographic profiles (Figures 2 and 7), and LayerTools dip analysis suggest that tilting of the plateaus and conical mounds was limited, possibly only to regions that were most proximal to the interchaos basins. From the topography data, the upper horizontal surfaces of some plateaus in western Iani Chaos are at an equal elevation to the surrounding highland terrain, while others in northern, central, and eastern Iani Chaos occur only a few hundred meters below the highlands (Figures 1 and 2). These observations confirm that significant collapse and subsurface volume loss did not occur beneath the basin-proximal plateaus and was restricted to only specific zones in Iani Chaos that correspond with the locations of the modern day, fracture-controlled interchaos basins.

[62] Given the observation of grooved flood terrains (Ares Vallis) that emanate from basins within Iani Chaos (B1–B4), we propose that volume loss within this region of the highlands was caused by the evacuation of previously confined groundwater. We suggest that Iani Chaos formed by collapse-induced extensional fracturing and basin formation over an aquifer that was pressurized beneath a thickened cryosphere [*Carr*, 1979; *Coleman et al.*, 2007; *Leask et al.*, 2006; *Lucchitta et al.*, 1994]. As hypothesized for other circum-Chryse chaotic terrains [*Anderson et al.*, 2001; *Dohm et al.*, 2001; *Komatsu et al.*, 2004; *Lucchitta et al.*, 1994; *Rodriguez et al.*, 2005a], the directional component of the chaos-related extensional fractures identified in northern and southern Iani Chaos may be consistent with the complex radial and concentric patterns of tectonic fracturing associated with the long-term evolution of the Tharsis bulge. There is some direct chronologic evidence to link the formation of global/regional fractures caused by the construction of Tharsis and opening of Valles Marineris to the initiation of flooding and groundwater release at Iani Chaos. Our absolute and relative chronology data indicate that basin formation in Iani Chaos likely occurred as early as the Hesperian (B3 and B4) and as late as the early Amazonian (B1, B2, B5). The initial construction of Tharsis in the Noachian and the opening of Valles Marineris after the late Noachian and into the Hesperian [*Anderson et al.*, 2001; *Anguita et al.*, 2006; *Carr and Head*, 2010; *Nimmo and Tanaka*, 2005; *Schultz*, 1998; *Tanaka et al.*, 1991; *Werner*, 2009] likely occurred before, or at the very beginning of, the initial early Hesperian flooding activity in Ares Vallis [*Warner et al.*, 2009, 2010]. Therefore, it is possible that

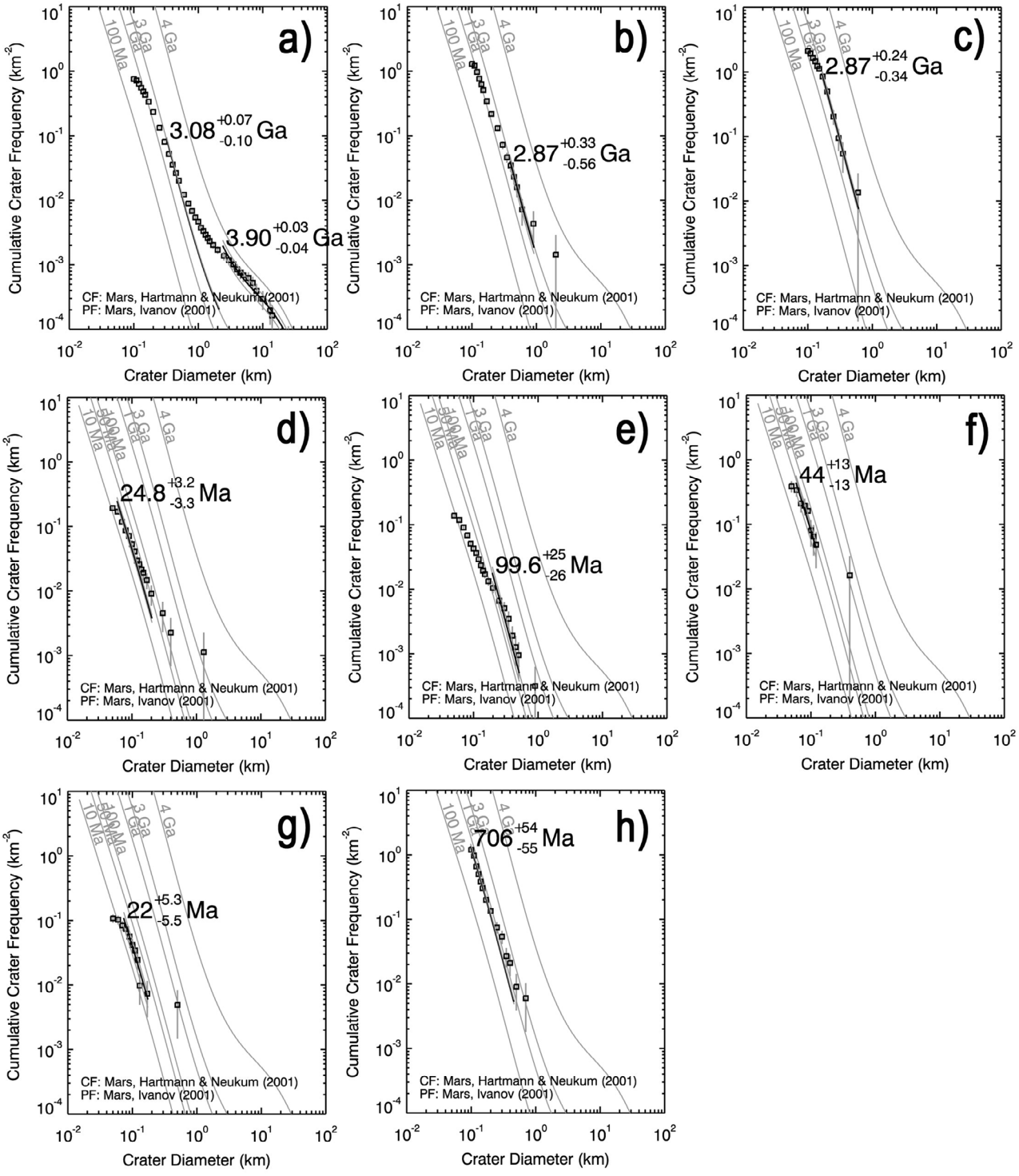

Figure 18. Cumulative frequency histograms for impact craters in Iani Chaos. The model ages are derived from specific surfaces that include (a) fractured highland plateaus, (b) infill within a floor-fractured crater, (c) interchaos grooved terrain (flood eroded), (d) ILD exposures in northern Iani Chaos (I1–I3), (e) ILDs in central Iani Chaos (I4), (f) ILDs in eastern Iani Chaos (I5), (g) ILDs in southern Iani Chaos (I6), and (h) the mantling unit.

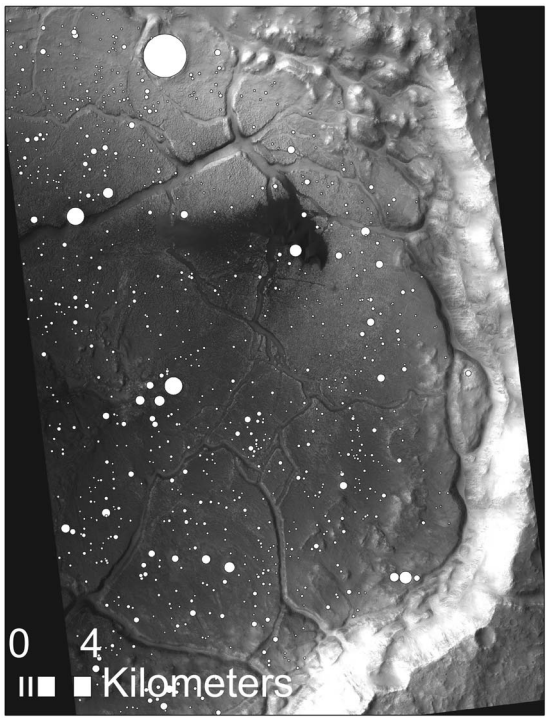

Figure 19. CTX image B03_010671_1759_XN_04S016W highlighting the craters on the floor of the infill material within a floor-fractured crater in southern Iani Chaos. The fractures crosscut the infill material. The crater statistics indicate a late Hesperian to early Amazonian age for the infill. This constrains the age of this fracturing event to some point after this time, suggesting that extensional fracturing in Iani Chaos may have occurred into the early Amazonian.

preexisting tectonic fractures, originating from a global Tharsis-related stress field, may have facilitated the release of water at Iani Chaos, acting as a point of weakness or permeable conduit through which pressurized subsurface water could escape.

4.2. Other Chaos Formation Hypotheses

[63] It has been proposed that impact crater floors may have represented initial zones of crustal weakness through which subsurface water could have gained access to the surface [*Sato et al.*, 2010]. The image and topography data indicate that the interchaos depressions, in most cases, do not exhibit diagnostic impact basin morphologies (circular planform morphology, raised rims, ejecta, conical central peaks). In fact, the largest semicircular basins (B1 and B2) contain central topographic highs that are significantly broad (up to 50 km in width), flat-topped, and heavily cratered. These characteristics are inconsistent in relative scale and morphology with the conical central peaks of large impact craters (Figures 1 and 2). Aside from the few preserved fractured floor craters in Iani Chaos (Figures 17 and 19), there is no confirming observational evidence that the largest chaos depressions are collapsed remnants of these features. However, it is unclear whether the fracture/basin alignments in Iani Chaos were generated by the occurrence of preexisting fractures associated with large, Noachian age, buried impact basins [*Rodriguez et al.*, 2005b]. Fractures associated with the crater containing Aram Chaos and with large crater basins south of Iani Chaos, including the Argyre, Ladon, and Margaritifer basins (among others) [*Grant and Parker*, 2002], may have had a control in generating a complex regional extensional stress field (in conjunction with, or separate from the Tharsis-related field) that facilitated water release at Iani Chaos. Similarly, from our observations we also reject the possibility that Iani Chaos and Ares Vallis formed from the release of pressurized, ice-covered lakes that were sustained within preexisting impact craters or topographic depressions [*Zegers et al.*, 2010]. If preexisting depressions existed, they were likely small and did not dominate the preexisting geomorphology of the region.

[64] The occurrence of chaotic terrains on the floors of some circum-Chryse flood channels has been proposed as evidence that flood erosion is capable of initiating chaos formation by removing bedrock overburden from a pressurized aquifer [*Coleman*, 2005; *Rodriguez et al.*, 2005a]. However, there is no evidence of flood grooving, channel systems, streamlined features, or other diagnostic indicators of catastrophic flooding on top of chaos blocks in Iani Chaos or within the interchaos basins, aside from the small grooved terrains adjacent to B3 and B4. Furthermore, while it has been proposed that

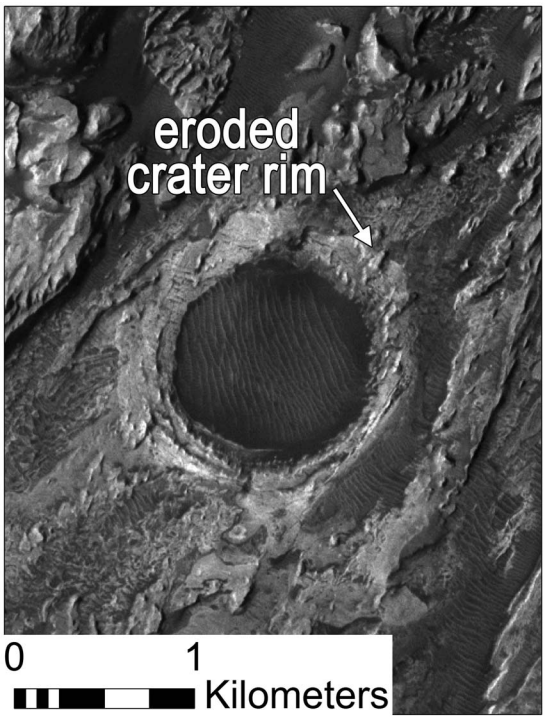

Figure 20. CTX image P04_002562_1795_XN_00S017W showing a 1 km size impact crater on the surface of an ILD deposit in northern Iani Chaos (I2). The crater is highly degraded and is superimposed by grooves that are likely associated with wind erosion. The morphology of the impact craters and the presence of yardang-like grooves on the ILDs indicate that the ILDs are easily eroded and likely semifriable. Crater statistics that are derived from the ILDs therefore can only provide a crater retention age and not the true formation age of the deposits.

the Margaritifer flood system may have entered directly into the southern region of Iani Chaos before the formation of Ares Vallis [*Grant and Parker*, 2002], we have not observed evidence in the high-resolution imagery for flood grooved terrain or channels that enter Iani. Rather, several interconnected chaos basins define the northern portion of the Margaritifer fluvial-chaos system.

[65] It remains unclear whether igneous processes caused initial deformation and fracturing of the highland crust or pressurization of subsurface water in the Iani Chaos region. Regional mean slope measurements (Figure 7) do not reveal evidence for regional deformation, such as doming, that may have been associated with upwelling magma. Furthermore, CTX imagery does not reveal conclusive evidence for surface volcanism or exhumed intrusive morphologies (e.g., dykes). While it is possible that regional intrusive processes may have initiated Iani Chaos, the frequency of flood activity within Ares Vallis [*Warner et al.*, 2009, 2010] would have required intrusive igneous activity to have occurred on multiple occasions throughout a period of ~1 Ga. Furthermore, evidence for time-synchronous flooding from Iani and Hydapsis Chaos (separated spatially by ~500 km) [*Warner et al.*, 2010] would have also required the circumstance of coincidental independent igneous activity that heated subsurface water or melted subsurface ice deposits beneath two different chaos locations. We therefore propose that the trigger mechanism for flooding likely involved a long-lived or episodic regional process that is difficult (but not impossible) to explain by a volcanic mechanism that left no obvious surface expression.

[66] Other origin hypotheses that include the release of groundwater during major impact events [*Wang et al.*, 2005], dissolution of subsurface hydrous clathrates [*Hoffman*, 2000; *Komatsu et al.*, 2000; *Max and Clifford*, 2001], and sublimation of an ice-rich substrate [*Pedersen and Head*, 2010] are difficult to assess from morphology alone. The likelihood that sufficiently large impact events could have generated sustained thermal energy to melt subsurface ice of sufficient volumes to catastrophically and episodically erode Ares Vallis throughout a period of ~1 Ga seems unlikely. Furthermore, if this hypothesis were correct, the impact event(s) did not leave obvious geomorphic markers. Figures 1 and 17 reveal three and possibly four obvious prechaos craters in Iani Chaos with D > 16 km (largest = 40 km) over an area of ~80,000 km^2. Large impact events were extremely rare during our proposed timing for chaos formation (Hesperian to early Amazonian) [*Hartmann*, 2005]. Late Hesperian age surfaces on Mars collected only ~10 impact craters with D > 16 km over an area of 10^6 km^2 (N(16)). For early Hesperian age surfaces, the N(16) value is ~20.

[67] Sublimation or dissolution of subsurface, hydrous materials (e.g., ice, sulfates, and clathrates) may have resulted in regionally restricted collapse events as is observed in Iani Chaos. Water that was derived from hydrous materials during dissolution may have been released through preexisting weaknesses in the crust as we propose for the interchaos basins. However, both the dissolution and sublimation hypotheses at Iani Chaos need to be reconciled with the association and catastrophic nature of flood channels and the implication that floods in Ares Vallis occurred on multiple occasions. It is also difficult to assess both the climatic conditions required to facilitate large-scale sublimation of an ice deposit beneath Iani Chaos or the chemical and stratigraphic relationships that would be required to dissolve enough hydrated minerals to release water of sufficient volume to erode Ares Vallis.

4.3. Multiple Collapse Episodes

[68] The minimum volume loss of material beneath Iani Chaos is on the order of 10^4 km^3, estimated from the HRSC DTM (Table 1). By comparison, *Warner et al.* [2009] identified bedrock terraces and flood-eroded trimlines within Ares Vallis that suggested water depths between 200 m and 500 m for individual flood events. Using the total area of the bedrock-eroded canyon system of Ares Vallis (~1.1×10^5 km^2) and assuming an estimated flood depth of 200 m, a rough, minimum total volume of material eroded by a single flood event in Ares Vallis is 2.0×10^4 km^3. This volume estimate excludes the distal region of Ares Vallis where the flood entered Chryse Planitia. In this region, volume is difficult to calculate as down-cutting was limited where the flood expanded. A total maximum volume for Ares Vallis, including the total depth of the channel systems is ~10^5 km^3.

[69] While the erodibility of the Martian terrain at Ares Vallis, flow viscosity, and flood sediment concentration are unknown, we suggest that the total volume loss within Iani Chaos (10^4 km^3) is insufficient to explain the erosion of Ares Vallis (10^4–10^5 km^3) by a single, turbulent water flood, derived from an isolated aquifer of equivalent volume to the chaos depressions. Furthermore, it is unlikely that the total volume loss in Iani Chaos can be accounted for by release of pure liquid water. Rather, some volume of material evacuated from the interchaos basins may have been sediment and/or ice. The total volume of water that was available from the basins to do erosive work in Ares Vallis was therefore likely less than the total estimated basin volumes. If floods of the equivalent volume to the interchaos basins carved Ares Vallis, then the sediment to water ratio (~1:1) of the floods would have been more similar to that of a viscous debris flow. On the basis of the geomorphology of putative flood deposits at the mouth of the circum-Chryse outflow channels, *Tanaka* [1999] suggested that the channels might have been carved by sediment-rich debris flows. However, by terrestrial analogy [*Baker and Nummedal*, 1978], the occurrence of longitudinal grooves, knickpoints (cataracts), streamlined islands, and terraced flood surfaces within Ares Vallis [*Warner et al.*, 2009] is more consistent with erosion by turbulent water floods. The channel-source volume disparity therefore requires the possibility that (1) water was recharged from distal sources into Iani Chaos and resulted in multiple flood events into Ares Vallis and/or (2) tributaries, including channels from Aram and Hydapsis Chaos, contributed some unknown volume of water to the erosion of Ares Vallis. Estimates for the total volume of Aram Chaos (10^4 km^3) [*Zegers et al.*, 2010] and Hydapsis Chaos (10^4 km^3) (our estimate) are of the same order of magnitude to the Iani Chaos basins. Taken together, and without a mechanism of water recharge, floods of this combined volume would still be characterized by a significantly high sediment to water ratio.

[70] Uncertainties in the amount of water released from tributaries to Ares Vallis make it difficult to assess whether their contribution alone could explain the erosion of Ares

Vallis. However, observations of multiple terraced surfaces in Ares Vallis upstream of these tributaries indicate that multiple floods likely issued directly from Iani Chaos [*Warner et al.*, 2009]. Furthermore, from our fracture and chaos-mound analysis, we have identified evidence for multiple, overlapping fracture events and superimposing chaos-mound morphologies that are indicative of fracturing related to extensional collapse at different spatial scales at different times (Figures 9 and 10). The occurrence of small conical mounds contained within shallow depressions, superimposed on the surfaces of larger chaos plateaus, represents one example of overlapping chaos formation events (Figure 10). We suggest that this morphology is best explained if older, shallow chaos depressions (similar in depth and morphology to B3 and B4) were later fractured by younger, kilometer-scale extensional features. By this model, the shallower depressions and conical mound morphology formed from localized, shallow subsidence, while the larger fractures resulted from regional extension that followed the formation of the deepest (up to 2 km) interchaos basins (B1–B2, B5–B8).

[71] In support of the multiple collapse hypothesis, we have identified grooved terrains and shallow chaos basins (including B3 and B4) along the northwest margin of Iani Chaos that are truncated by (and are therefore older than) the deeper basins B1 and B5 (Figures 2 and 3 and Table 1). B3 and B4 occur directly adjacent to flood terrain and we suggest that some of these shallow basins may represent the direct source of the small flood events. By comparison, B1, which destroys the margins of the shallow basins, truncates the youngest, early Amazonian age Ares Vallis flood surface (S6, Table 2), suggesting that collapse of B1 was one of the last major events in the region. These relative relationships require multiple overlapping collapse events that are associated with multiple, topographically distinct flood channels.

4.4. Hypotheses for Observed Basin and Fracture Chronology

[72] Assuming the model of cryosphere overpressurization for the initiation of flooding into Ares Vallis, the relative chronology of fracturing and basin formation events in Iani Chaos may suggest a temporal control on the depth of collapse that was created by conditions within the cryosphere. We envision two possible scenarios for the observed cross-cutting fracture and basin relationships that indicate that the deepest chaos basins are preceded by shallower collapse events.

[73] 1. Early-stage (early Hesperian), shallow (200–500 m) collapse events involved only small volumes of water. This water was sourced from a deep (~2 km) aquifer that was pressurized by overburden of a thickened cryosphere. The shallow collapse events occurred in the initial stage of cryosphere weakening/fracturing as water permeated through fractures in the cryosphere. Shallow collapse by this mechanism may have occurred owing to local subsidence over the evacuated zone. Later events (Hesperian to early Amazonian) were more catastrophic, owing to further cracking of the cryosphere and opening of the aquifer to the surface. Multiple water release events may have been facilitated by not only recharge of groundwater into the system but refreezing of the fractures and aquifer repressurization [*Andrews-Hanna and Phillips*, 2007; *Hanna and Phillips*, 2006; *Wang et al.*, 2006]. The younger water release events in this scenario tapped larger volumes of water and thus caused deeper collapses and regional extension.

[74] 2. Early-stage (early Hesperian) shallow collapse events resulted from the release of water from a shallow subsurface water source, beneath a thin cryosphere (200 m–500 m). With time, progressive deepening of the cryosphere and water source led to overpressurization and deep-seated collapse events, forming younger, 1 to 2 km deep collapse depressions in the late Hesperian to early Amazonian.

[75] The intriguing possibility of scenario 2 is that the observed pattern of overlapping fractures and basins was generated by cooling of the global climate from the early Hesperian into the early Amazonian. This cooling would have thickened the regionally extensive cryosphere beneath Iani Chaos, causing the groundwater release events (floods) to tap a source that deepened with time. If this model is correct, chaos morphology may be a proxy for understanding the evolution of the Hesperian hydro/cryosphere, with the implication that the cryosphere thickened beneath Iani Chaos from 200 m to 2 km from the early Hesperian into the early Amazonian.

4.5. Distal Groundwater Recharge

[76] Given the source-channel volume disparity, the chronology of the flood system, our observations for discrete basins, and the topographic evidence for limited subsidence beneath the fractured highlands, we suggest that episodic effusion of water into Ares Vallis was controlled by distal water recharge that was not derived from local sources within the general region of Iani Chaos. While the water was likely vertically confined beneath a cryosphere, it was directed laterally through a regionally connected fracture-controlled subsurface aquifer system with episodic water release events occurring at the sites of specific zones of crustal weakness. By this model, water release is spatially restricted to specific release points where multiple floods may have occurred following cycles of repeated aquifer freezing and overpressurization [*Andrews-Hanna and Phillips*, 2007; *Hanna and Phillips*, 2006; *Harrison and Grimm*, 2008; *Rodriguez et al.*, 2005a; *Wang et al.*, 2006]. Because the fractured highlands that are adjacent to the collapse basins in Iani Chaos show limited warping/tilting and exhibit equivalent elevation to the highland terrain, they may overlie a completely intact, deep, frozen aquifer that was untapped by flooding events. Alternatively, the aquifer may have been compartmentalized [*Harrison and Grimm*, 2009] and present only along specific regions of high crustal permeability (e.g., fracture systems). Northward and eastward directed subsurface flow out of Iani Chaos is implied by the orientation of the chaos-proximal flood channels. Recharge of this system may have been possible if the subsurface aquifer was interconnected with distal aquifer systems associated with other chaotic terrains east of Vallis Marineris or with chaotic terrains and basins located south of Iani Chaos, including Margaritifer Chaos and Ladon Basin [*Grant and Parker*, 2002].

4.6. Relationship of ILD Formation to the Chaos Terrain

[77] From observed onlapping relationships of the ILDs with chaos blocks in THEMIS-VIS images, *Glotch and Rogers* [2007] and *Dobrea et al.* [2008] suggested that ILD deposi-

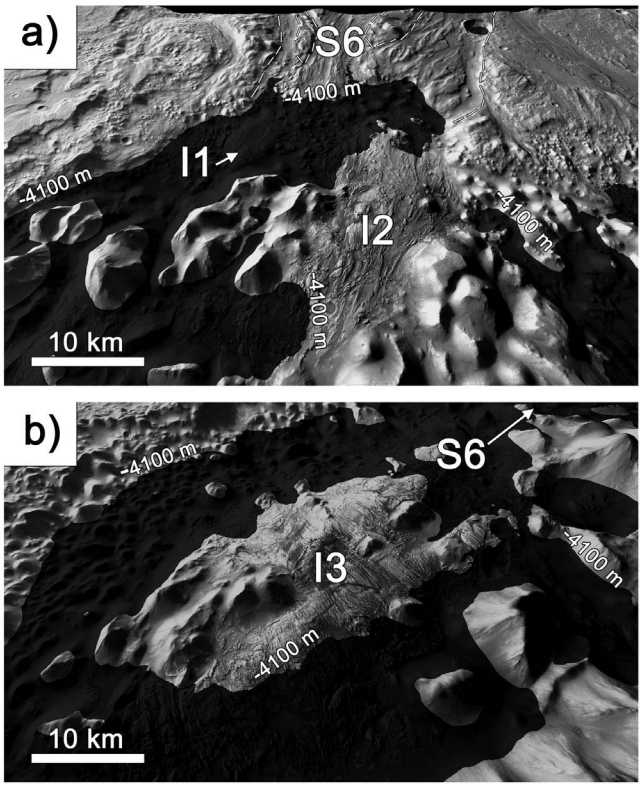

Figure 21. Perspective HRSC views of northern Iani Chaos displaying important topographic relationships of the ILDs and the flood channels of Ares Vallis. (a) The mean elevation of the proximal surface of S6 (youngest Ares Vallis flood channel) is approximately −4100 m. This image displays the −4100 m contour across the northwestern region of B1. The upper surface of I2 rests approximately 350 m above the −4100 m contour. This suggests that any water surface (a lake) that was contained within this contour was not of sufficient elevation to account for deposition of the upper surface of I2. (b) Along the western margin of B1, I3 rests approximately 400 m above the −4100 m contour. This also suggests that water confined behind S6 could not account for deposition of the upper surface of I3.

tion generally occurred after formation of the chaotic terrain. These observations are consistent with the results of our analysis, obtained from higher resolution CTX images and HRSC-derived topography data (Figures 13–15). On the basis of relative associations with previous crater count statistics of the Ares Vallis region [*Rotto and Tanaka*, 1995; *Tanaka et al.*, 2003], *Glotch and Rogers* [2007] suggested a scenario that the sulfate and hematite-bearing ILDs that overly the chaotic terrain formed in the Hesperian, after and/or during catastrophic flooding in Ares Vallis. These authors proposed that multiple smaller floods, derived from Iani Chaos, may have resulted in the formation of playa lake environments within isolated, semienclosed basins, correlating with the basins B1–B8. Model-based predictions of late-stage, low-magnitude floods from Iani Chaos have been used to suggest that ponding may have occurred within preexisting collapse depressions where sulfate-hematite mineralization occurred in an evaporative lake environment [*Andrews-Hanna and Phillips*, 2007].

[78] Our updated chronology data and topographic observations presented in this analysis enable us to (1) constrain the timing of ILD formation in Iani Chaos and (2) test the hypothesis that the ILDs were deposited within lacustrine environments that were generated after the chaos basins were formed. The crater statistics for the ILDs (Figures 18d–18g) suggest a late Amazonian crater-retention age. This result is similar to the crater statistics study presented by *Rossi et al.* [2008], who supplied a late Amazonian crater retention age of 0.3 Ma for a limited area of the Iani Chaos ILDs, including the deposits in the northern and southern regions of the chaotic terrain. From image observations, the surfaces of most of the ILDs are grooved and show poor crater preservation with superposition of the grooves on the rims of the current crater population (Figures 13, 15, and 20). This suggests that grooving of the ILDs is likely the result of a recent, late Amazonian process. The pattern of surface grooving is clearly not consistent with erosion by floods, as the groove orientations are variable and do not typically show a consistent orientation relative to local slope and flooding in Ares Vallis. Furthermore, chaos blocks that surround the ILDs lack a streamlined morphology that would suggest significant erosion by water (Figure 15). Rather, the grooved morphology on all ILD surfaces is likely the result of relatively recent wind erosion, with local variations in orientation caused by diversion of winds around complex topography. By this mechanism, the grooves are yardangs that formed within a semifriable material.

[79] The late Amazonian model age for the ILDs is either (1) a crater retention age that represents the time since the surface of the ILDs has become stable enough to allow for the establishment of a crater population or (2) an exhumation age that indicates the time since the ILDs have been exposed to cratering. Our image analysis reveals a regionally extensive mantling unit across Iani Chaos (Figure 16). This mantling unit overlies and embays chaos mounds and fractures, occurs at variable elevations, and has been eroded in places to form scarps that expose underlying light-toned ILDs (Figures 13d and 16c). From crater statistics collected from a continuous patch of the mantling unit in northern Iani Chaos, we have obtained a middle Amazonian model age (Figure 18h). It is therefore likely that the ILDs within Iani Chaos predate the mantling unit and that their youthful crater model age may represent the time since exhumation from beneath the mantling unit.

[80] From CTX image observations it is clear that all the major ILD outcrops (I1–I6) rest on top of chaos mounds and superimpose both large and small fracture systems (Figures 13 and 15). This indicates that the ILDs were deposited after Iani Chaos was fully developed, after basins B1–B8 were formed. From crosscutting relationships between the flood grooves of the proximal channels in Ares Vallis and the interior walls of B1–B2 (Figure 11), we suggest that these basins (containing I1–I3) formed after the final flood erosional event in Ares Vallis. Using the crater statistical analysis presented by *Warner et al.* [2009, 2010] (Table 2), and these relative associations, we can constrain the timing of formation for the ILDs in B1 and B2 to sometime in the

Amazonian, after the early Amazonian flood events that formed the topographically lowest channels of Ares Vallis. For the ILDs in B5–B8, we lack relative chronologic information because there is no direct contact between flood channels of Ares Vallis and the basin walls. However, because many of these deposits underlie the regionally extensive mantling unit, they likely formed at some time after chaos formation and before the middle Amazonian.

[81] From the topographic observations presented in section 3.1.6 (Figure 14) we have determined that not all the analyzed ILD outcrops correspond with the topographically lowest regions in Iani Chaos. Most importantly, aside from I1, the upper surfaces of all the major ILDs (I2–I6) are topographically higher than the lowest flood channels of Ares Vallis (S5, S6). In the case of I2, which occurs only a few kilometers south of the proximal reach of S6, its upper surface lies ~350 m above the floor of the flood channel (Figures 2b and 21a). From this simple topographic observation, and the observation that I2 must have formed after B1 and thus after the proximal flood channels of Ares Vallis, we suggest that it is impossible for I2 to have formed by sedimentary deposition or evaporative accumulation within a standing body of water within B1. Given the relative chronology, we suggest that at the time of deposition of layered units in I2, there was no topographic boundary high enough that could have supported the formation of an equipotential lake surface within B1 to allow for deposition of the uppermost layered unit of the ILD mound. Similarly, the highest layered unit exposed within I3 is ~420 m higher than the proximal channels of Ares Vallis (Figure 21b). For I4–I6, topographic barriers are lacking where preexisting large fracture systems crosscut the surrounding basin walls. In order for standing water to have covered the topographically highest ILD (I4), water would have also inundated most of the interchaos fractures and depressions that predate formation of I4. This would have generated a massive interchaos lake system; however, we do not observe any geomorphologic or topographic indicators of a regionally extensive lake.

[82] Our results require an alternative formation mechanism to the lacustrine basin hypothesis for the ILDs in Iani Chaos. Recently, *Rossi et al.* [2008] presented a scenario for the Amazonian age deposition of the ILDs in Iani Chaos as spring deposits. By this model, upwelling acidic waters, flowing through preexisting chaos fractures, deposited mound-like, sulfate-bearing layered units. Our analysis indicates that this scenario may be more plausible for the Iani Chaos ILDs than the lacustrine hypothesis. However, the origin of this Amazonian age water reservoir is unclear. In an alternative model, air fall deposition by aeolian or volcanic processes may have generated regionally extensive, terrain-blanketing stacks of horizontally layered materials that were later altered by aqueous processes and partially eroded by wind, removing evidence of these deposits on upper surfaces of the chaotic terrains. The air fall deposition model however does not account for the fact that some of the topographically lowest, confined regions in Iani Chaos, which are possibly the areas that are protected by wind erosion, do not contain evidence for ILD deposition. The exact origin mechanism for the ILDs in Iani Chaos remains unresolved and requires higher resolution analysis (e.g., HiRISE images and DTMs) to identify lateral and vertical patterns in the stratigraphy of the deposits that might identify a specific process.

4.7. Summary of Geologic History of Iani Chaos

[83] Figure 22 provides a schematic summary that illustrates our proposed relative and absolute sequence of events for the formation of Iani Chaos as it relates to collapse events, fracturing, and flooding within Ares Vallis. The schematic highlights the uncertainties about the depth of the subsurface aquifer/cryosphere during the long-term evolution of Iani Chaos. Either a constant depth aquifer model or progressive aquifer deepening model can explain the observed features in Iani Chaos if the volume of individual water effusion events is adjusted to account for shallow collapses with the deep aquifer model. Below, we highlight some of the major events that formed Iani Chaos and describe important interpretations.

[84] 1. The first event in this region is identified in the crater statistics from the nonfractured highland terrain that surrounds Iani Chaos. Deposition of the horizontally layered units that comprise the surface of the highland terrain and the fractured plateaus occurred in the late Noachian, near 3.9 Ga (Table 2).

[85] 2. Crater statistics from the topographically highest, shallow flood surfaces in Ares Vallis reveal a flood resurfacing age of ~3.6 Ga [*Warner et al.*, 2009]. This suggests that evacuation of water from the Iani Chaos region may have begun as soon as the early Hesperian. Shallow collapse depressions (e.g., B3 and B4) and densely fractured mounds that superimpose larger fractured plateaus may represent the source of these earliest floods.

[86] 3. The shape of the cumulative frequency curve in Figure 18a indicates a resurfacing event on the highlands and on the fractured plateaus during the Hesperian, at ~3.0 Ga. The origin of this resurfacing is enigmatic. It is unclear from this data set whether fracturing within Iani Chaos occurred before, during, or after the resurfacing, as the process of resurfacing may have additionally affected the interiors of the fractures. This would particularly be relevant if top-down erosion or burial (air fall) removed craters across the entire region.

[87] 4. A limited set of crater statistics identified a late Hesperian age flood event (~3.0 Ga) on the small grooved terrains associated with B3 and B4 on the northwest margin of Iani Chaos. On the basis of crosscutting relationships, both the flood surfaces and the basins formed before B1 and B5 and before the topographically lowest flood channels of Ares Vallis (S5, S6).

[88] 5. Impact crater statistics taken from the topographically lowest flood channels in Ares Vallis (S5, S6) indicate a early Amazonian flood resurfacing age of ~2.5 Ga – 2.9 Ga [*Warner et al.*, 2009, 2010]. These surfaces represent the last major flood erosional activity within Ares Vallis.

[89] 6. The northern rims of B1 and B2 truncate flood grooves and smooth surfaces associated with S5 and S6. This indicates that these large interchaos basins, in their current form, formed at some time after the early Amazonian (<2.5 Ga – 2.9 Ga).

[90] 7. ILDs throughout Iani Chaos rest unconformably on top of chaos mounds suggesting that they formed after Iani Chaos was fully developed. From relative relationships with the youngest Ares Vallis flood channels, the ILDs in B1 and B2 must have formed at some point after the early Amazonian (<2.5 Ga – 2.9 Ga).

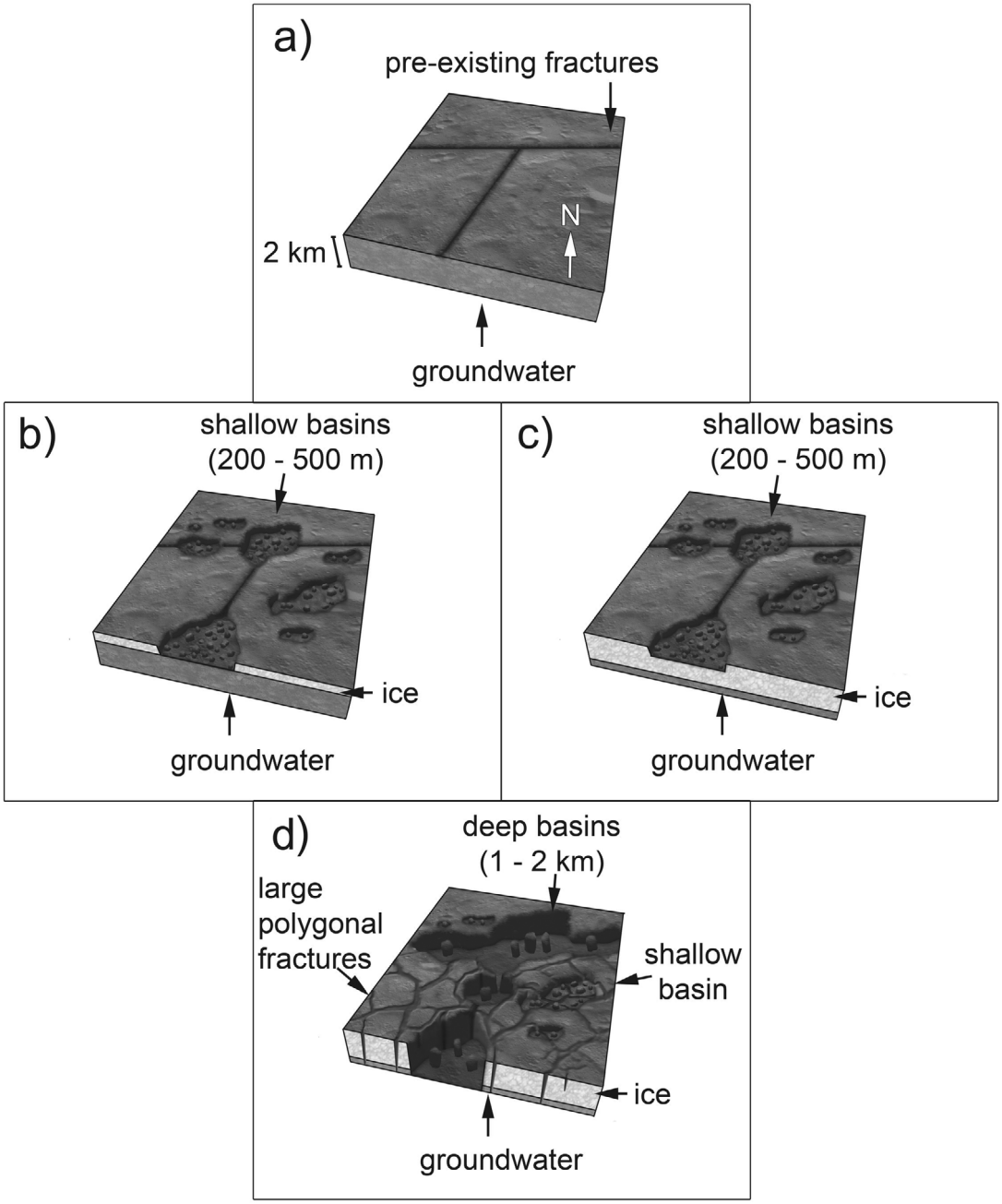

Figure 22. Schematic 3-D diagram displaying our proposed time sequence of chaos formation at Iani Chaos. (a) Preexisting fractures with a general NNE-SSW and ENE-WSW orientation were present within the highlands at the site of Iani Chaos. Groundwater was likely present to some unknown depth beneath the surface. (b) In the early Hesperian, the upper 200–500 m of the groundwater table was frozen. Low-volume, pressurized release of groundwater from beneath the thin ice occurred along and adjacent to the fracture systems. This release led to shallow collapse events and low-volume floods. (c) Alternatively to the model in Figure 22b, in the early Hesperian the liquid water aquifer was trapped beneath 1 to 2 km of ice. Pressurized release of small volumes of water from this deep aquifer led to shallow collapse events. (d) In the Hesperian and into the early Amazonian, pressurized release of large volumes of water from a deep (1–2 km) aquifer led to catastrophic floods and deep collapse events, forming large interchaos basins. Regional-scale extensional fracture systems developed in the highland marginal regions. Many of the fractures trend parallel to the basins and crosscut the older, shallower interchaos basins.

[91] 8. A regional mantling deposit drapes chaos mounds and ILDs throughout the entire Iani Chaos region and extends into Margaritifer and Meridiani Terra. From a crater statistics study of a continuous patch of the mantling deposit, we suggest the mantle formed during the middle Amazonian (~700 Ma). The extent and draping characteristics of the mantle point to an air fall origin.

[92] 9. Late Amazonian (<100 Ma) aeolian erosion and/or exhumation of the ILDs in Iani Chaos resulted in the establishment of a new crater population on the ILDs.

5. Conclusion

[93] In this analysis we have provided constraints for the origin and long-term evolution of Iani Chaos. Our results demonstrate the following: (1) Collapse of the highland crust in the Iani Chaos region was limited to specific locations that correspond to interchaos basins. (2) The interchaos basins formed by volume loss within the subsurface, likely related to groundwater effusion. (3) The total measured volume of the interchaos basins is not sufficient to explain the erosion of Ares Vallis by a single water flood event. (4) Collapse of the highland terrain led to regional and local extension that created polygonal fracture systems. (5) Multiple overlapping fracture sets suggest multiple episodes of collapse. (6) The extensional fractures and associated basins form nonrandom patterns that require a preexisting control on the location of collapse and water release. (7) Preexisting weaknesses in the crust, generated by an extensional stress field associated with Tharsis, may have both caused the observed alignments of the interchaos basins and allowed recharge of groundwater from distal sources through the Iani Chaos region. (8) ILDs are present within and adjacent to the interchaos basins, but not necessarily at the topographically lowest points in Iani Chaos. (9) ILDs are younger than the basins they are contained within and the basins that border flood terrains in Ares Vallis are younger than the flooding events. (10) Lakes of sufficient depth to deposit the ILDs could not have been sustained within the basins given the lack of bounding topography.

[94] The impact crater statistics and relative chronologies indicate that Iani Chaos formed during the Hesperian, with basin formation continuing into the early Amazonian. Our chronology for this chaos region is generally consistent with the timing of erosion within the associated flood channels of Ares Vallis [*Marchenko et al.*, 1998; *Nelson and Greeley*, 1999; *Rotto and Tanaka*, 1995; *Tanaka and Skinner*, 2004; *Warner et al.*, 2009, 2010]. We suggest that the long-lived flood erosion history that has been proposed for Ares Vallis [*Warner et al.*, 2009, 2010] was likely controlled by multiple groundwater effusion events, followed by episodes of collapse and fracturing of the highland terrain at Iani Chaos. Furthermore, these results require that groundwater was present (possibly episodically) beneath the Iani Chaos region for a significant period of Mars history (~1 Ga), with recharge occurring from distal sources. Variations in the depths of the interchaos basins (200 m – 2 km) may be caused by either (1) differences in the volume of material that was evacuated from a deep aquifer (~1 km to 2 km) or (2) deepening of the aquifer through time. The aquifer-deepening hypothesis requires further testing, but may explain the observed relative chronology in Iani Chaos, where shallow chaos depressions are crosscut by the margins of deeper basins. By this model, the geologic evolution of Iani Chaos may have been controlled by climate cooling during the Hesperian and Amazonian when thickening of the cryosphere generated deeper, pressurized aquifer systems.

[95] **Acknowledgments.** We thank the HRSC PI, Gerhard Neukum (Freie Universitaet Berlin), and the team at the German Aerospace Centre (DLR) in Berlin as well as ESA for use of the HRSC data and various preprocessing software. We also thank the NASA MRO project and the CTX and HiRISE teams for use of their data. This research is supported by the UK STFC (Science and Technology Facilities Council) under grants ST/F003099/1 and PP/E002366/1. S.G. was supported by a Royal Society–Leverhulme Trust Senior Research Fellowship. Kristy Barkan (Academy of Art University, San Francisco) is thanked for creating Figure 22. We would like to thank Alexis Rodriguez and Keith Harrison for their thorough reviews.

References

Anderson, R. C., J. M. Dohm, M. P. Golombek, A. F. C. Haldemann, B. J. Franklin, K. L. Tanaka, J. Lias, and B. Peer (2001), Primary centers and secondary concentrations of tectonic activity through time in the western hemisphere of Mars, *J. Geophys. Res.*, *106*(E9), 20,563–20,585, doi:10.1029/2000JE001278.

Andrews-Hanna, J. C., and R. J. Phillips (2007), Hydrological modeling of outflow channels and chaos regions on Mars, *J. Geophys. Res.*, *112*, E08001, doi:10.1029/2006JE002881.

Anguita, F., C. Fernandez, G. Cordero, S. Carrasquilla, J. Anguita, A. Nunez, S. Rodriguez, and J. Garcia (2006), Evidences for a Noachian-Hesperian orogeny in Mars, *Icarus*, *185*(2), 331–357, doi:10.1016/j.icarus.2006.07.026.

Baker, V. R. (1982), *The Channels of Mars*, Univ. of Tex. Press, Austin.

Baker, V. R., and R. C. Kochel (1979), Martian channel morphology: Maja and Kasei Valles, *J. Geophys. Res.*, *84*(B14), 7961–7983, doi:10.1029/JB084iB14p07961.

Baker, V., and D. J. Milton (1974), Erosion by catastrophic floods on Mars and Earth, *Icarus*, *23*(1), 27–41, doi:10.1016/0019-1035(74)90101-8.

Baker, V. R., and D. Nummedal (Eds.) (1978), *The Channeled Scablands*, 186 pp., NASA, Washington, D.C.

Baker, V. R., R. G. Strom, V. C. Gulick, J. S. Kargel, G. Komatsu, and V. S. Kale (1991), Ancient oceans, ice sheets and the hydrological cycle on Mars, *Nature*, *352*(6336), 589–594, doi:10.1038/352589a0.

Carr, M. H. (1979), Formation of Martian flood features by release of water from confined aquifers, *J. Geophys. Res.*, *84*(B6), 2995–3007, doi:10.1029/JB084iB06p02995.

Carr, M. (1996), *Water on Mars*, 229 pp., Oxford Univ. Press, New York.

Carr, M. H., and J. W. Head (2010), Geologic history of Mars, *Earth Planet. Sci. Lett.*, *294*(3–4), 185–203, doi:10.1016/j.epsl.2009.06.042.

Chapman, M. G., and K. L. Tanaka (2002), Related magma-ice interactions: Possible origins of chasmata, chaos, and surface materials in Xanthe, Margaritifer, and Meridiani Terrae, Mars, *Icarus*, *155*(2), 324–339, doi:10.1006/icar.2001.6735.

Chapman, M. G., M. T. Gudmundsson, A. J. Russell, and T. M. Hare (2003), Possible Juventae Chasma subice volcanic eruptions and Maja Valles ice outburst floods on Mars: Implications of Mars Global Surveyor crater densities, geomorphology, and topography, *J. Geophys. Res.*, *108*(E10), 5113, doi:10.1029/2002JE002009.

Coleman, N. M. (2005), Martian megaflood-triggered chaos formation, revealing groundwater depth, cryosphere thickness, and crustal heat flux, *J. Geophys. Res.*, *110*, E12S20, doi:10.1029/2005JE002419.

Coleman, N. M., C. L. Dinwiddie, and K. Casteel (2007), High outflow channels on Mars indicate Hesperian recharge at low latitudes and the presence of Canyon Lakes, *Icarus*, *189*(2), 344–361, doi:10.1016/j.icarus.2007.01.020.

Dobrea, E. Z. N., F. Poulet, and M. C. Malin (2008), Correlations between hematite and sulfates in the chaotic terrain east of Valles Marineris, *Icarus*, *193*(2), 516–534, doi:10.1016/j.icarus.2007.06.029.

Dohm, J. M., J. C. Ferris, V. R. Baker, R. C. Anderson, T. M. Hare, R. G. Strom, N. G. Barlow, K. L. Tanaka, J. E. Klemaszewski, and D. H. Scott (2001), Ancient drainage basin of the Tharsis region, Mars: Potential source for outflow channel systems and putative oceans or paleolakes, *J. Geophys. Res.*, *106*(E12), 32,943–32,958, doi:10.1029/2000JE001468.

Gendrin, A., et al. (2005), Suffates in Martian layered terrains: The OMEGA/Mars Express view, *Science*, *307*(5715), 1587–1591, doi:10.1126/science.1109087.

Glotch, T. D., and P. R. Christensen (2005), Geologic and mineralogic mapping of Aram Chaos: Evidence for a water-rich history, *J. Geophys. Res.*, *110*, E09006, doi:10.1029/2004JE002389.

Glotch, T. D., and A. D. Rogers (2007), Evidence for aqueous deposition of hematite- and sulfate-rich light-toned layered deposits in Aureum and Iani Chaos, Mars, *J. Geophys. Res.*, *112*, E06001, doi:10.1029/2006JE002863.

Grant, J. A., and T. J. Parker (2002), Drainage evolution in the Margaritifer Sinus region, Mars, *J. Geophys. Res.*, *107*(E9), 5066, doi:10.1029/2001JE001678.

Hanna, J. C., and R. J. Phillips (2006), Tectonic pressurization of aquifers in the formation of Mangala and Athabasca Valles, Mars, *J. Geophys. Res.*, *111*, E03003, doi:10.1029/2005JE002546.

Harrison, K. P., and R. E. Grimm (2008), Multiple flooding events in Martian outflow channels, *J. Geophys. Res.*, *113*, E02002, doi:10.1029/2007JE002951.

Harrison, K. P., and R. E. Grimm (2009), Regionally compartmented groundwater flow on Mars, *J. Geophys. Res.*, *114*, E04004, doi:10.1029/2008JE003300.

Hartmann, W. K. (2005), Martian cratering 8: Isochron refinement and the chronology of Mars, *Icarus*, *174*(2), 294–320, doi:10.1016/j.icarus.2004.11.023.

Hartmann, W. K., and G. Neukum (2001), Cratering chronology and the evolution of Mars, *Space Sci. Rev.*, *96*, 165–194, doi:10.1023/A:1011945222010.

Hoffman, N. (2000), White Mars: A new model for Mars' surface and atmosphere based on CO2, *Icarus*, *146*(2), 326–342, doi:10.1006/icar.2000.6398.

Ivanov, B. A. (2001), Mars/Moon cratering rate ratio estimates, *Space Sci. Rev.*, *96*, 87–104, doi:10.1023/A:1011941121102.

Kargel, J. S., R. Furfaro, O. Prieto-Ballesteros, J. A. P. Rodriguez, D. R. Montgomery, A. R. Gillespie, G. M. Marion, and S. E. Wood (2007), Martian hydrogeology sustained by thermally insulating gas and salt hydrates, *Geology*, *35*(11), 975–978, doi:10.1130/G23783A.1.

Kim, J.-R., and J.-P. Muller (2009), Multi-resolution topographic data extraction from Martian stereo imagery, *Planet. Space Sci.*, *57*, 2095–2112, doi:10.1016/j.pss.2009.09.024.

Kneissl, T., S. van Gasselt, and G. Neukum (2010), Measurement of strike and dip of geologic layers from remote sensing data: New software tool for ArcGIS, *Proc. Lunar Planet. Sci. Conf.*, *41st*, 1640.

Komatsu, G., and V. R. Baker (1997), Paleohydrology and flood geomorphology of Ares Vallis, *J. Geophys. Res.*, *102*(E2), 4151–4160, doi:10.1029/96JE02564.

Komatsu, G., J. Kargel, V. R. Baker, R. G. Strom, G. G. Ori, C. Mosangini, and K. L. Tanaka (2000), A chaotic terrain formation hypothesis: Explosive outgas and outflow by dissociation of clathrate on Mars, *Proc. Lunar Planet. Sci. Conf.*, *31st*, 1434.

Komatsu, G., J. M. Dohm, and T. M. Hare (2004), Hydrogeologic processes of large-scale tectonomagmatic complexes in Mongolia-southern Siberia and on Mars, *Geology*, *32*(4), 325–328, doi:10.1130/G20237.2.

Leask, H. J., L. Wilson, and K. L. Mitchell (2006), Formation of Aromatum Chaos, Mars: Morphological development as a result of volcano-ice interactions, *J. Geophys. Res.*, *111*, E08071, doi:10.1029/2005JE002549.

Lucchitta, B. K., N. K. Isbell, and A. Howingtonkraus (1994), Topography of Valles-Marineris: Implications for erosional and structural history, *J. Geophys. Res.*, *99*(E2), 3783–3798, doi:10.1029/93JE03095.

Marchenko, A. G., A. T. Basilevsky, H. Hoffman, E. Hauber, A. C. Cook, and G. Neukum (1998), Geology of the common mouth of the Ares and Tiu Valles, Mars, *Sol. Syst. Res.*, *32*, 425–452.

Masursky, H., J. M. Boyce, A. L. Dial, G. G. Schaber, and M. E. Strobell (1977), Classification and time of formation of Martian channels based on Viking data, *J. Geophys. Res.*, *82*(28), 4016–4038, doi:10.1029/JS082i028p04016.

Max, M. D., and S. M. Clifford (2001), Initiation of Martian outflow channels: Related to the dissociation of gas hydrate?, *Geophys. Res. Lett.*, *28*(9), 1787–1790, doi:10.1029/2000GL011606.

Maxwell, T. A., and M. D. Picard (1974), Evidence of subsurface water in equatorial region of Mars, *AAPG Bull.*, *58*, 915.

Meresse, S., F. Costard, N. Mangold, P. Masson, G. Neukum, and the HRSC Co-I Team (2008), Formation and evolution of the chaotic terrains by subsidence and magmatism: Hydraotes Chaos, Mars, *Icarus*, *194*(2), 487–500, doi:10.1016/j.icarus.2007.10.023.

Michael, G., and G. Neukum (2008), Surface dating: Software tool for analysing crater sizefrequency distributions including those showing partial resurfacing events, *Proc. Lunar Planet. Sci. Conf.*, *39th*, 1780.

Michael, G. G., and G. Neukum (2010), Planetary surface dating from crater size-frequency distribution measurements: Partial resurfacing events and statistical age uncertainty, *Earth Planet. Sci. Lett.*, *294*(3–4), 223–229, doi:10.1016/j.epsl.2009.12.041.

Montgomery, D. R., and A. Gillespie (2005), Formation of Martian outflow channels by catastrophic dewatering of evaporite deposits, *Geology*, *33*(8), 625–628, doi:10.1130/G21270.1.

Nelson, D. M., and R. Greeley (1999), Geology of Xanthe Terra outflow channels and the Mars Pathfinder landing site, *J. Geophys. Res.*, *104*(E4), 8653–8669, doi:10.1029/98JE01900.

Nimmo, F., and K. Tanaka (2005), Early crustal evolution of mars, *Annu. Rev. Earth Planet. Sci.*, *33*, 133–161, doi:10.1146/annurev.earth.33.092203.122637.

Ori, G. G., and C. Mosangini (1998), Complex depositional systems in Hydraotes Chaos, Mars: An example of sedimentary process interactions in the Martian hydrological cycle, *J. Geophys. Res.*, *103*(E10), 22,713–22,723, doi:10.1029/98JE01969.

Pedersen, G. B. M., and J. W. Head (2010), Chaos formation by sublimation of volatile-rich substrate: Evidence from Galaxias Chaos, Mars, *Icarus*, *211*(1), 316–329.

Rodriguez, J. A. P., S. Sasaki, and H. Miyamoto (2003), Nature and hydrological relevance of the Shalbatana complex underground cavernous system, *Geophys. Res. Lett.*, *30*(6), 1304, doi:10.1029/2002GL016547.

Rodriguez, J. A. P., S. Sasaki, R. O. Kuzmin, J. M. Dohm, K. L. Tanaka, H. Miyamoto, K. Kurita, G. Komatsu, A. G. Fairen, and J. C. Ferris (2005a), Outflow channel sources, reactivation, and chaos formation, Xanthe Terra, Mars, *Icarus*, *175*(1), 36–57, doi:10.1016/j.icarus.2004.10.025.

Rodriguez, J. A. P., et al. (2005b), Control of impact crater fracture systems on subsurface hydrology, ground subsidence, and collapse, Mars, *J. Geophys. Res.*, *110*, E06003, doi:10.1029/2004JE002365.

Rossi, A. P., G. Neukum, M. Pondrelli, S. van Gasselt, T. Zegers, E. Hauber, A. Chicarro, and B. Foing (2008), Large-scale spring deposits on Mars?, *J. Geophys. Res.*, *113*, E08016, doi:10.1029/2007JE003062.

Rotto, S., and K. L. Tanaka (1995), Geologic/geomorphic map of the Chryse Plantatia region, *U.S. Geol. Surv. Misc. Geol. Invest. Map*, *I-2441*.

Sato, H., K. Kurita, and D. Baratoux (2010), The formation of floor-fractured craters in Xanthe Terra, *Icarus*, *207*(1), 248–264, doi:10.1016/j.icarus.2009.10.023.

Schultz, R. A. (1998), Multiple-process origin of Valles Marineris basins and troughs, Mars, *Planet. Space Sci.*, *46*, 827–829, doi:10.1016/S0032-0633(98)00030-0.

Scott, D. H., and K. Tanaka (1986), Geologic map of the western equatorial region of Mars, *U.S. Geol. Surv. Misc. Geol. Invest. Map*, *I-1802-A*.

Sharp, R. P. (1973), Mars: Fretted and chaotic terrains, *J. Geophys. Res.*, *78*(20), 4073–4083, doi:10.1029/JB078i020p04073.

Simpson, J. I., J. R. Kim, and J.-P. Muller (2008), 3D crater database production on Mars by automated crater detection and data fusion, paper presented at ISPRS Congress Beijing 2008, Int. Soc. for Photogramm. and Remote Sens., Beijing.

Tanaka, K. L. (1997), Sedimentary history and mass flow structures of Chryse and Acidalia Planitiae, Mars, *J. Geophys. Res.*, *102*(E2), 4131–4149, doi:10.1029/96JE02862.

Tanaka, K. L. (1999), Debris-flow origin for the Simud/Tiu deposit on Mars, *J. Geophys. Res.*, *104*(E4), 8637–8652, doi:10.1029/98JE02552.

Tanaka, K. L., and J. A. Skinner (2004), Advances in reconstructing the geologic history of the Chryse region outflow channels on Mars, *Proc. Lunar Planet. Sci. Conf.*, *35th*, *1770*.

Tanaka, K. L., M. P. Golombek, and W. B. Banerdt (1991), Reconciliation of stress and structural histories of the Tharsis region of Mars, *J. Geophys. Res.*, *96*(E1), 15,617–15,633, doi:10.1029/91JE01194.

Tanaka, K. L., J. A. Skinner, T. M. Hare, T. Joyal, and A. Wenker (2003), Resurfacing history of the northern plains of Mars based on geologic mapping of Mars Global Surveyor data, *J. Geophys. Res.*, *108*(E4), 8043, doi:10.1029/2002JE001908.

Tanaka, K., J. A. Skinner, and T. M. Hare (2005), Geologic map of the Northern Plains of Mars, *U.S. Geol. Surv. Misc. Geol. Invest. Map*, *SIM-2888*.

Wang, C. Y., M. Manga, and A. Wong (2005), Floods on Mars released from groundwater by impact, *Icarus*, *175*(2), 551–555, doi:10.1016/j.icarus.2004.12.003.

Wang, C. Y., M. Manga, and J. C. Hanna (2006), Can freezing cause floods on Mars?, *Geophys. Res. Lett.*, *33*, L20202, doi:10.1029/2006GL027471.

Warner, N., S. Gupta, J. P. Muller, J. R. Kim, and S. Y. Lin (2009), A refined chronology of catastrophic outflow events in Ares Vallis, Mars, *Earth Planet. Sci. Lett.*, *288*(1–2), 58–69, doi:10.1016/j.epsl.2009.09.008.

Warner, N. H., S. Gupta, J. R. Kim, S. Y. Lin, and J. P. Muller (2010), Retreat of a giant cataract in a long-lived (3.7–2.6 Ga) Martian outflow channel, *Geology*, *38*(9), 791–794, doi:10.1130/G31268.1.

Werner, S. C. (2009), The global Martian volcanic evolutionary history, *Icarus*, *201*(1), 44–68, doi:10.1016/j.icarus.2008.12.019.

Williams, R. M., R. J. Phillips, and M. C. Malin (2000), Flow rates and duration within Kasei Valles, Mars: Implications for the formation of a Martian ocean, *Geophys. Res. Lett.*, *27*(7), 1073–1076, doi:10.1029/1999GL010957.

Zegers, T. E., J. H. P. Oosthoek, A. P. Rossi, J. K. Blom, and S. Schumacher (2010), Melt and collapse of buried water ice: An alternative hypothesis for the formation of chaotic terrains on Mars, *Earth Planet. Sci. Lett.*, *297*(3–4), 496–504, doi:10.1016/j.epsl.2010.06.049.

S. Gupta, C. McGonigle, and N. H. Warner, Department of Earth Science and Engineering, Imperial College London, South Kensington Campus, London SW7 2AZ, UK. (n.warner@imperial.ac.uk)

J.-R. Kim, Department of Geoinformatics, University of Seoul, Dongdeamun-gu, Seoul 130-743, Korea.

L. Le Corre and J.-P. Muller, Mullard Space Science Laboratory, Department of Space and Climate Physics, University College London, Holmbury St. Mary RH5 6NT, UK.

S.-Y. Lin, Department of Land Economics, National Chengchi University, ZhiNan Road, Taipei, 11605 Taiwan.

J. Morley, Centre for Geospatial Science, Sir Clive Granger Building, University of Nottingham, University Park, Nottingham NG7 2RD, UK.